Manuscript prepared for Atmos. Chem. Phys.
with version 2015/04/24 7.83 Copernicus papers of the LaTeX class copernicus.cls.
Date: 4 May 2016

Impact of the Asian monsoon on the extratropical lower stratosphere: Trace gas observations during TACTS over Europe 2012

S. Müller[1], P. Hoor[1], H. Bozem[1], E. Gute[2,a], B. Vogel[3], A. Zahn[4], H. Bönisch[5], T. Keber[5], M. Krämer[3], C. Rolf[3], M. Riese[3], H. Schlager[6], and A. Engel[5]

[1]Institute for Atmospheric Physics, Johannes Gutenberg-University, Mainz, Germany
[2]Department of Atmospheric Chemistry, Max Planck Institute for Chemistry, Mainz, Germany
[3]Institute for Energy and Climate Research - Stratosphere (IEK-7), Forschungszentrum Jülich, Jülich, Germany
[4]Institute of Meteorology and Climate Research (IMK), Karlsruhe Institute of Technology (KIT), Karlsruhe, Germany
[5]Institute for Atmospheric and Environmental Sciences, Goethe-University of Frankfurt, Frankfurt am Main, Germany
[6]Institute for Atmospheric Physics, German Aerospace Research Center (DLR), Oberpfaffenhofen, Germany
[a]now at: Department of Chemistry, University of Toronto, Toronto, Canada

Correspondence to: Stefan Müller
(stefan.mueller@uni-mainz.de)

Abstract. The transport of air masses originating from the Asian monsoon anticyclone into the extratropical upper troposphere and lower stratosphere (Ex-UTLS) above potential temperatures Θ = 380 K was identified during the HALO aircraft mission TACTS in August and September 2012. In-situ measurements of CO, O_3 and N_2O during TACTS Flight 2 on the 30 August 2012 show the irreversible mixing of aged with younger (originating from the troposphere) stratospheric air masses within the Ex-UTLS. Backward trajectories calculated with the trajectory module of the CLaMS model indicate that these tropospherically affected air masses originate from the Asian monsoon anticyclone. These air masses are subsequently transported above potential temperatures $\Theta = 380$ K from the monsoon circulation region into the Ex-UTLS where they subsequently mix with stratospheric air masses. The overall trace gas distribution measured during TACTS shows that this transport pathway had a significant impact on the Ex-UTLS during boreal summer and autumn 2012. This leads to an intensification of the tropospheric influence on the extratropical lower stratosphere with PV > 8 pvu within three weeks during the TACTS mission. During the same time period a weakening of the tropospheric influence on the lowermost stratosphere (LMS) is determined. The study shows that the transport of air masses originating from the Asian summer monsoon region within the lower stratosphere is of major importance for the change of the chemical composition of the Ex-UTLS and significantly contributes to the flushing of the LMS during summer 2012.

1 Introduction

The impact of air masses originating from the Asian monsoon anticyclone on the trace gas composition of the upper troposphere / lower stratosphere (UTLS) has not yet been quantified and is only poorly known. The UTLS region (Fig.1) encompasses the global tropopause region and the lower part of the stratosphere up to potential temperature levels of $\Theta = 430\,\mathrm{K}$ which coincides with the lower end of the tropical pipe in the stratosphere (e.g. Hegglin and Shepherd, 2009; Palazzi et al., 2009). Transport in the UTLS is thus affected by the stratospheric Brewer-Dobson circulation (BDC, Brewer, 1949; Dobson, 1956) with slow diabatic ascent in the tropics across the tropical tropopause layer (TTL) (Fueglistaler et al., 2009) and diabatic downwelling in the extratropical stratosphere. The BDC consists of two significant different transport pathways. The deep branch of the BDC transports air from the tropics to the extratropics via the upper stratosphere and lower mesosphere on time scales of several years (Butchart, 2014). In contrast, the shallow branch of the BDC mainly affects the region between $\Theta = 380\,\mathrm{K}$ and $430\,\mathrm{K}$ by quasi-isentropic transport and mixing (Hegglin and Shepherd, 2007; Spackman et al., 2007; James and Legras, 2009; Birner and Bönisch, 2011). On the basis of in-situ data Volk et al. (1996) and (Flocke et al., 1999) quantified entrainment rates for the tropical stratosphere highlighting the importance of mixing above $\Theta = 380\,\mathrm{K}$ for the ascending part of the BDC. In the extratropics below $\Theta = 380\,\mathrm{K}$ the lowermost stratosphere (LMS) (Hoskins et al., 1985) as part of the extratropical UTLS (Ex-UTLS in the following) is affected by rapid isentropic transport and mixing across the subtropical jet. Transport across the extratropical tropopause layer (ExTL) further potentially contributes to the composition of the lower part of the Ex-UTLS. The ExTL and LMS are mainly characterized by exchange processes across the tropopause on time scales of days to weeks (Berthet et al., 2007; Bönisch et al., 2009; Hoor et al., 2010; Konopka and Pan, 2012; Jurkat et al., 2014). A detailed knowledge of the relative strength of these transport pathways is of major importance to quantify the chemical composition of the Ex-UTLS, which in turn determines the radiative, dynamical and chemical impact of this atmospheric region on the climate system (Forster and Shine, 2002; Riese et al., 2012).

As shown in Bönisch et al. (2009) and Ploeger et al. (2013) the seasonality of stratospheric transport processes above $\Theta = 380\,\mathrm{K}$ leads to a seasonality of the chemical composition up to $\Theta = 430\,\mathrm{K}$ (the bottom of the tropical pipe) and a "flushing" of the lower stratosphere with young tropical air masses up to this level in summer and autumn (Hegglin and Shepherd, 2007). In this context, the Asian summer monsoon is an important pathway for the transport of tropospheric constituents into the stratosphere and has gained increasing attention in atmospheric research (Randel and Park, 2006; Randel et al., 2010; Park et al., 2007, 2008, 2009; Bergman et al., 2013; Fadnavis et al., 2013, 2014, 2015). The Asian summer monsoon consists of a cyclonic flow and convergence in the lower troposphere and a large scale anticyclonic circulation in the upper troposphere between June and September centered over southern Asia (Randel et al., 2010). This circulation pattern is coupled with persistent deep convection (Bourassa et al., 2012; Bergman et al., 2013) which lifts chemical

constituents from the lower troposphere to the tropopause region and lower stratosphere (Randel et al., 2010). Therefore, water vapour and tropospheric trace gases as carbon monoxide (CO) and methane (CH_4) are relatively high within the Asian monsoon anticyclone (Rosenlof et al., 1997; Park et al., 2004, 2007), whereas ozone (O_3) is relatively low (Park et al., 2008). The air within the Asian monsoon anticyclone is strongly affected by anthropogenic pollution, which originates from east Asian and Indian densly populated regions. During summer these pollutants accumulate in the anticyclone (Schuck et al., 2010; Baker et al., 2011; Richter et al., 2005) and strongly perturb the chemical composition of the monsoon tropopause region (Glatthor et al., 2009).

Since the monsoon tropopause is relatively high (Highwood and Hoskins, 1998), exchange processes between the troposphere and stratosphere in the region of the Asian monsoon may transport tropospheric constituents into the lower stratosphere to altitudes up to 20 km (Park et al., 2008). The pathway and strength of troposphere-to-stratosphere-transport (TST) in the tropopause region of the Asian monsoon are neither adequately understood nor quantified. In this context, the direct convective injection into the lower stratosphere (Rosenlof et al., 1997; Chen et al., 2012) and the separation of small anticyclones from the main anticyclone, so called “eddy shedding“, is of major importance (Hsu and Plumb, 2000; Popovic and Plumb, 2001; Garny and Randel, 2013). The latter process can transport tropospheric trace gases and pollutants to mid- and high latitudes, where they mix with extratropical stratospheric air masses (Vogel et al., 2014). The impact of the Asian monsoon on the chemical composition of the northern hemispheric lower stratosphere cannot easily be separated from the upward transport of tropospheric air masses into the stratosphere in the tropics, which is regarded as the primary pathway for air masses entering the stratosphere (Holton et al., 1995). In the tropical lower stratosphere these ascending air masses are uplifted by the Brewer-Dobson circulation and zonally transported to higher latitudes by the shallow branch of the BDC.

In this paper we present in-situ trace gas measurements of CO, N_2O (nitrous oxide), and O_3 in the northern hemisphere extratropical stratosphere up to potential temperatures $\Theta = 410\,\mathrm{K}$ obtained during the TACTS (Transport and Composition in the Upper Troposphere and Lower Stratosphere) aircraft campaign. The measurements are combined with analysis data of the European Centre for Medium-Range Weather Forecast (ECMWF) and backward trajectories calculated with the trajectory module of the Chemical Lagrangian Model of the Stratosphere (CLaMS) (McKenna et al., 2002a, b; Konopka et al., 2010; Pommrich et al., 2014).

We will focus on the impact of tropospheric air from the monsoon region on the composition of the lower stratosphere on different timescales. “Young stratospheric" in this context denotes air masses, which are clearly located in the stratosphere from a dynamical and chemical point of view, but which still exhibit chemical signatures of previous tropospheric influence (e.g. CO mixing ratios larger than the CO equilibrium mixing ratio of chemically processed (aged) stratospheric air masses of $\mathrm{CO} = 12.5 \pm 2.5$ ppbv (Herman et al., 1999; Flocke et al., 1999). Since the measurements were performed in boreal summer and autumn 2012 within a period of four weeks in a wide range of the

northern hemispheric UTLS, the potential influence of the Asian monsoon on this transport pathway and therefore on the trace gas composition of the Ex-UTLS is studied. In the following we will use the term lower stratosphere (LS), when we refer to the stratospheric part of the Ex-UTLS. This refers to the lower stratosphere above the ExTL up to $\Theta = 430$ K, which is different from the classical definition of the LMS.

The paper is organised as follows: Section 2 gives an overview of the measurements and methods applied. Section 3 presents a case study of TACTS-Flight 2 (30 August 2012), which illustrates the identification of irreversible mixing of young stratospheric air masses into the extratropical stratosphere above $\Theta = 380$ K. Tracer-tracer-scatterplots of TACTS-Flight 2 are analysed in Sect. 3.2. Section 3.3 shows the results of backward trajectory calculations, which indicate that transport and mixing from the Asian monsoon anticyclone into the Ex-UTLS cause the measured mixing event. In section 4 we will provide strong evidence that the Asian summer monsoon strongly affected the mid-latitude lower stratosphere in summer 2012. A summary and discussion of the results (Sec. 5) and a conclusion (Sec. 6) closes the paper.

2 Project overview, measurements, and backward trajectory calculation

2.1 The TACTS campaign 2012

Our study is based on in-situ measurements performed during the first atmospheric science missions with the new German research aircraft HALO in August / September 2012 TACTS (Transport and Composition of the UTLS) and ESMVal (Earth System Model Vaildation). This paper focuses on eight research flights covering the Ex-UTLS between 15N to 70N and 25W to 15E with typically 8-10 hours per flight (see supplement).

The measurements of TACTS can be subdivided into two phases. The first phase with approx. 35 flights hours covered the time period between the 30 August and 5 September 2012. The end phase was performed from the 23 September until 26 September 2012. The flights, which are the basis for our study, were performed between 200 hPa and 130 hPa up to $\Theta = 410$ K. The composition change in the Ex-UTLS between both phases will be compared in section 4. As shown in the supplement, the flights were performed mainly in regions of horizontal PV-gradients associated with Rossby wave activity. During both phases the flights covered a region from the Cape Verdes to the Arctic. PV values exceeding 10 pvu during both phases clearly indicate, that stratospheric air masses were probed during TACTS.

2.2 In-situ trace gas measurements

The study is mainly based on in-situ data from the TRIHOP (CO and N_2O) and FAIRO (O_3) instrument aboard HALO as described in the following subsections. Basic meteorological and avionic data

are taken from the Basic HALO Measurement and Sensor System (BAHAMAS). For the following analysis all data are merged to one dataset with a time resolution of 10 s (0.1 Hz), corresponding to a horizontal resolution of 2.5 km.

2.2.1 TRIHOP in-situ measurements of CO and N_2O

The TRIHOP instrument is a three channel Quantum Cascade Laser Infrared Absorption spectrometer that measured CO, and N_2O during TACTS and ESMVal 2012 (Schiller et al., 2008). The instrument applies Quantum Cascade Laser Absorption Spectroscopy (QCLAS) in the mid-infrared with a multipass absorption cell (type White), which is kept at a constant pressure of P = 30 hPa and has a path length of 64 m and a volume of 2.7 l. During TACTS / ESMVal the instrument was in-situ calibrated approx. every 30 minutes during the flights against a secondary standard of compressed ambient air. The mixing ratios of the secondary standard were determined before and after the campaign in the laboratory against National Oceanic and Atmospheric Administration (NOAA) standards. The in-flight calibrations are used to identify and correct slow instrumental drifts in the post-flight data evaluation. The integration time for each species was 1.5 s at a duty cycle of 8 s, which limits the temporal resolution of the measurements. During TACTS and ESMVal TRIHOP CO (N_2O) data achieved a 2σ precision of 1.0 (1.1) ppbv and a stability of the instrument of 1.5 (2.2) ppbv before applying the post flight data correction. Note that the stability is based on the mean drift between two subsequent calibrations, which were performed in intervals of 30 minutes during the flights. These instrumental drifts are corrected after the flights assuming linear drift, which leads to a reduced uncertainty. Hence, the total uncertainty relative to the working standard of 1.8 (2.5) ppbv can be regarded as an upper limit.

2.2.2 FAIRO in-situ measurements of O_3

FAIRO is a new accurate ozone instrument developed for use on board the HALO aircraft. It combines two techniques, the UV photometry (light absorption of O_3 at λ = 250 - 260 nm) with high accuracy and chemiluminescence detection with high measurement frequency. A UV-LED is used as a light source for the UV photometer, which can be controlled well (in contrast to Hg lamps) for constant light emission. The 1-sigma precision is 0.08 ppbv at a measurement frequency of 4 s and a cuvette pressure of 1 bar and the total uncertainty is 2%. The chemiluminescence detector shows a measurement frequency of 12.5 Hz and a precision of 0.05 ppbv (at 10 ppbv absolute, a measurement frequency of 5 Hz, and a pressure of 1 bar) (Zahn et al., 2012).

2.3 ECMWF (meteorological data)

Global meteorological analysis data (T1279L91) of the ECMWF (European Centre for Medium-Range Weather Forecast) are used to interpret the meteorological situation during TACTS Flight

2 as shown in Sect. 3.1. The meteorological fields are available every 3 hours interpolated onto a regular grid of 0.5° horizontal spacing.

2.4 CLaMS-TRAJ (backward trajectories)

The trajectory module CLaMS-TRAJ of the Chemical Lagrangian Model for the Stratosphere (CLaMS) is used to calculate backward trajectories at the positions of the in-situ observations (McKenna et al., 2002a, b; Konopka et al., 2010; Pommrich et al., 2014). The trajectories are initialised every 10 seconds along the flight paths and calculated 50 days back in time. For this purpose ERA-Interim reanalysis data (Dee et al., 2011) with a resolution of 1° and 60 vertical levels from the surface up to 0.1 hPa are interpolated in time and space on the starting point of the backward trajectories. Meteorological data, e.g. pressure, temperature, altitude, Θ and potential vorticity (PV) are available every 1 hour along the backward trajectories. The horizontal motion of the trajectories are driven by horizontal winds from the ERA-Interim reanalysis data. Diabatic heating rates are used to calculate vertical velocities in the UTLS region for pressure levels lower than 300 hPa (Ploeger et al., 2010). Below P $>$ 300 hPa a pressure-based hybrid vertical coordinate is applied (Pommrich et al., 2014).

3 Case study: TACTS Flight 2 on 30 August 2012

TACTS flight 2 on 30 August 2012 was performed over western Europe and the eastern Atlantic with departure and landing in Oberpfaffenhofen near Munich (see Fig. 2). An eastward propagating trough over western Europe was crossed several times on pressure levels between 220 and 130 hPa equivalent to flight altitudes between 11.5 and 15 km. On the highest flight levels on 150 and 130 hPa, air masses with potential temperatures Θ between 380 and 410 K were sampled. Potential vorticity (PV) derived from ECMWF data ranges between 8 and 14 pvu for these flight sections (Fig. 2(a) and (b)). Hence, these air masses are located above the dynamical tropopause, which is typically defined by PV-values from 1-4 pvu in the extratropics (Hoskins et al., 1985; Randel et al., 2007). In the subtropics above $\Theta = 340$ K, PV at the tropopause varies between 2 and 5 pvu (Kunz et al., 2011).

3.1 Irreversible mixing within the stratosphere

The time series of in-situ O_3, CO and pressure data for TACTS Flight 2 are shown in Fig.2(c). The CO data indicates three sections with mixing ratios lower than 40 ppbv during the flight, which is below CO mixing ratios in the northern hemispheric free troposphere ranging from 50 to 130 ppbv (Kumar et al., 2013). This indicates that the respective flight sections were within the stratosphere. Accompanying ozone values exceeding 200 ppbv (Strahan, 1999) and PV values larger than 5 pvu (cf. Fig. 2) support this conclusion.

During the last two flight segments from 10:30 until 12:15 UTC and 13:00 until 14:00 UTC, stratospheric air masses with CO ranging from 20 to 30 ppbv were sampled. These values are larger than the stratospheric equilibrium of CO = 12.5 $\pm$ 2.5 ppbv which establishes as a result of CO production from methane and chemical degradation of CO on the time scale of several months (Flocke et al., 1999). Therefore, CO between 20 and 30 ppbv indicates neither pure tropospheric nor completely CO degraded stratospheric air masses. Instead, such mixing ratios are the result of either irreversible mixing of tropospheric with stratospheric air or from the CO degradation of a former tropospheric air mass in the stratosphere (or a combination of both). In the following the correlation of CO with O_3 during TACTS Flight 2 is analysed to further examine the tropospheric influence in the Ex-UTLS for Θ between 380 and 410 K.

Without any exchange between the troposphere and stratosphere, the CO-O_3-scatterplot would form an L-shape (Fischer et al., 2000). Irreversible mixing of tropospheric (characterised by low O_3) and stratospheric (characterised by low CO) air masses appear as „mixing lines“, which connect the mixed reservoirs on the tracer-tracer-scatterplot (Hoor et al., 2002). Previous studies used the method of mixing lines to investigate exchange processes between the troposphere and stratosphere within the extratropical tropopause layer (ExTL) (Zahn et al., 2000; Hoor et al., 2004; Pan, 2004). As shown in Fig.3 (a) the observations indicate irreversible mixing above Θ = 380 K. Since this is above the middleworld isentropic cross tropopause mixing is most likely not the driving mechanism for the observed mixing lines. Low CO and high O_3 are accompanied by high values of Θ. From the fact that all CO data points are well above the stratospheric equilibrium of CO = 12.5 $\pm$ 2.5 ppbv (Herman et al., 1999; Flocke et al., 1999), tropospheric influence on time scales of weeks can be deduced for all probed air masses.

During TACTS Flight 2, five mixing lines (ML) at potential temperatures $\Theta \geq$ 380 K can be identified. These are marked by individual colors in Fig. 3 (b). The respective colors in Fig. 2 mark the location of the measured mixing lines on the flight path (Fig.2 (a) and (b)) and along the time series of CO and O_3 (Fig.2 (c)). ML 1, 2, 4, 5 were encountered in the center of the trough (Fig. 2 (a)), ML 3 is sampled at the trough edge further south. The five mixing lines correspond to individual flight sections along the flight track with durations of typically 15 minutes for each mixing line (see Fig. 2(c)). Table 1 lists the minimum and maximum values of CO, O_3 and Θ for each individual mixing line. Also shown are the number of data points, the flight distance, and R^2 from a linear fit regression for the respective mixing line. The applied fit is based on Press et al. (1992) and accounts for errors in both, x- and y-direction. The observed CO and O_3 range (CO: $>$ 4 ppbv, O_3: $>$ 60 ppbv) of each mixing line is larger than the total measurement uncertainty of both species. Therefore, measurement artefacts causing these mixing lines can be excluded. $R^2 \geq 0.89$ indicates that linearity for all mixing lines is justified. In general, ML 3 constitutes of higher CO and lower O_3 mixing ratios and exhibits a larger difference between the minimum and maximum values of both species compared to ML 1, 2, 4, 5. Significantly larger CO mixing ratios up to 40 ppbv compared to CO $<$ 30 ppbv for ML 1,

2, 4, 5 in combination with a higher tropospheric endmember (see Sect. 3.2) indicate shorter time scales for the transport and mixing of CO rich air masses from the troposphere into the stratosphere for ML 3 compared to the other mixing events. The fact that ML 3 is measured at the trough edge and at lower potential temperatures compared to ML 1 ,2, 4, 5 supports the assumption that different time scales are responsible for the formation of ML 3 and ML 1, 2 4, 5. In the following section the origin of the CO enhanced air masses in the extratropical lower stratosphere is further investigated with N_2O as an additional in-situ measured trace gas.

3.2 Mixing line analysis

This analysis seeks to determine the initial mixing ratios of the air parcels, which lead to the formation of mixing lines (Hintsa et al., 1998; Hoor et al., 2002). This requires knowledge on the initial mixing ratio of one of the species involved. Since mixing ratios of trace gases like O_3 and N_2O at the tropopause are fairly constant compared to their stratospheric gradient, they can be used to as initial estimate to analyze mixing across the tropopause. Nevertheless, mixing ratios just below the the tropopause of trace gases like O_3 and N_2O are fairly constant compared to their stratospheric gradient. Thus, the determination of the so called „tropospheric endmember“ is possible with the assumption of a constant tropospheric value for one of the constituents involved. This approach has been applied to ML 1-5 on the basis of the CO-O_3- and N_2O-CO-scatter plot.

Figure 4 displays the tropospheric endmember approximation for ML 4. The calculation of the shaded confidence region is based on the FITEXY-approach described by Press et al. (1992), which accounts for uncertainties in x- and y-direction. O_3 at the tropopause varies between 60 and 120 ppbv, with a seasonal cycle and regional variations as well. For the endmember approximation in this section a mixing ratio O_{3Trop} = 100 ppbv is applied, which is a reasonable value for the northern hemispheric summer (Zahn and Brenninkmeijer, 2003; Thouret et al., 2006). Alternatively, N_2O can be used to determine a tropospheric endmember. Superior to O_3, N_2O is inert in the troposphere and thus has an almost homogeneous distribution in the global troposphere. The sinks of N_2O are entirely in the stratosphere, which leads to a weak gradient of N_2O at the tropopause. Therefore, the N_2O mixing ratio at the tropopause is well defined, which makes N_2O an appropriate tracer for tropospheric air masses (Assonov et al., 2013; Müller et al., 2015). In August / September 2012 the free tropospheric mixing ratio of N_2O was 325 ± 0.5 ppbv, which is applied as N_2O_{Trop} (www.esrl.noaa.gov/gmd/hats/combined/N2O.html). Table 2 lists the potential range of the tropospheric endmember of CO from the calculated confidence region (shaded area in Fig. 4) for O_{3Trop} = 100 ppbv and N_2O_{Trop} = 325 ppbv, respectively. The results can be summarised as follows:

- The tropospheric endmembers of CO for ML 1, 2, 4, 5 are in a range from 35 to 55 ppbv. This is at the lower limit and even below typical tropospheric CO mixing ratios.

– Endmembers of CO based on the CO-O_3-correlation are different from the respective N_2O-CO-endmembers.

– CO endmembers between 55 and 70 ppbv for ML 3 includes typical mixing ratios at the tropopause, even though CO is at the lower limit for tropospheric CO mixing ratios.

A tropospheric CO endmember lower than typical tropopause values indicates that the respective mixing line is not the result of mixing between pure tropospheric and stratospheric air masses. (The term „pure" is used in this context to describe undiluted and photochemically unprocessed tropospheric air masses.) For these mixing lines the tropospheric CO endmembers do not reflect the original CO mixing ratio of the unmixed air mass. CO endmember values lower than the range of CO mixing ratios at the tropoapuse can only arise from the chemical degradation of CO in the stratosphere or previous mixing or a combination of both. Therefore, the observed mixing lines are the result of mixing between two stratospheric air masses with different age. Note that O_3 variability (and chemistry) in the lower stratosphere leads to differences in the tropospheric endmembers of CO based on the CO-O_3- and N_2O-CO-correlation. Thus, the formation of ML 1, 2, 4, 5 can only be caused by the irreversible mixing of stratospheric air masses with different age. In contrast, ML 3 indicates the irreversible mixing of pure tropospheric and stratospheric air masses.

These findings are supported by the meteorological situation and location where the mixing lines were measured. Air masses that form ML 1, 2, 4, 5 are probed in the centre of a trough far away from the jetstream (see Fig. 2). Since strong convective activity was absent during the flights fast transport of tropospheric air masses up to $\Theta = 400$ K can be ruled out. ML 3 arises, in contrast to the other mixing lines, presumably as a consequence of the irreversible mixing of tropospheric and stratospheric air masses at the jet stream, since this mixing event is measured at the edge of the trough in a region with high windspeed and windshear (Pan et al., 2006).

3.3 Results of backward trajectory calculations

We investigate the origin of ML 1, 2, 4, and 5, which were observed in the trough away from sharp isentropic PV gradients at the tropopause, by analyzing 50-day backward trajectories calculated with the CLaMS model. Variations of potential temperature Θ along the backward trajectories indicate diabatic processes in the history of the respective air masses. Figure 5 shows measured potential temperature Θ along TACTS Flight 2 (30 August 2012) color coded with PV from ECMWF analysis data. Black dots indicate the maximum potential temperature along each individual backward trajectory. These values are typically 20 K higher than the potential temperature at the position of the aircraft. This is in accordance with descending air masses in the extratropical stratosphere with a rate of approx. 0.5 K/day (Butchart, 2014). Red dots indicate the minimum Θ for trajectories which show a diabatic ascent prior to the time of measurement. These trajectories are primarily associated with

air masses showing large PV values ($>$ 8 pvu) in regions where the mixing lines were encountered. This finding provides an indication that diabatic upward transport of tropospherically influenced air masses is reflected by the diabatic ascent of the backward trajectories. Figure 6 displays those trajectories which show a potential temperature increase exceeding 5 K. These trajectories indicate an origin in the anticyclone of the Asian summer monsoon and subsequent transport to the measurement region in the Ex-UTLS above $\Theta = 400$ K. The position of the respective trajectories for -50 days $<$ t_{Tra} $<$ -30 days in Fig. 7 shows that a large fraction of the air masses is located within the Asian monsoon anticyclone for t_{Tra} $<$ -30 days. The lowest potential temperatures along the trajectories (bluish colors) appear within the Asian monsoon region. As shown in Fig. 8 the trajectories spend a significant amount of time in the region, which is affected by the Asian monsoon anticyclone. The location of the anticyclone shows a large variability within the two months prior to the measurements (see supplement) extending from 20 N to 45 N during some periods. The longest residence time of trajectories (Fig. 8) is however found in those regions which can be associated with the core region of the Asian monsoon anticyclone (Bergman et al., 2013; Garny and Randel, 2015).

The backward trajectory calculation suggests that the diabatic ascent within the Asian monsoon transports tropospheric air masses up to altitudes between 16 and 18 km. Figure 9 shows that this process is accompanied by PV values rising above 5 pvu and Θ larger 400 K. These air masses are subsequently transported at $t \approx$ -30 days to the extratropics were they mix with aged stratospheric air masses (as measured).

The calculation of 50-day back trajectories cannot provide unambiguous evidence that the transport of air masses from the Asian monsoon into the Ex-UTLS causes the occurence of mixing lines on the CO-O_3-correlation. CLaMS calculates the vertical motion using diabatic heating rates from ERA-Interim, which tend to have a relatively small vertical dispersion in the stratosphere compared to kinematic scenarios (Ploeger et al., 2010). Notably, Vogel et al. (2014) show that 40-day back trajectories, calculated with the same setup of CLaMS as used in this study, agree with trace gas measurements during TACTS Flight 6.

Trace gas measurements of TACTS Flight 2 and 50-day back trajectories are consistent, since CO-O_3 mixing lines indicate mixing at $\Theta > 380$ K. Endmember analysis shows that recent mixing at the tropopause cannot explain these mixing lines. The mixed air masses rather have experienced a significant CO degradation in the stratosphere. CLaMS trajectory calculations confirm this conclusion, since a transport time of $t \approx 30$ days from the Asian monsoon region into the Ex-UTLS is indicated by the backward trajectories. A significant contribution from the TTL for this region for TACTS Flight 2 cannot be identified based on the trajectory calculations. Thus, it is concluded that the Asian monsoon affects the trace gas composition of the Ex-UTLS for $\Theta > 380$ K during TACTS Flight 2.

4 Diagnosis of monsoon transport in the extratropical lower stratosphere

The effect of the Asian monsoon on the trace gas composition of the Ex-UTLS is investigated by comparing the changes of N_2O, CO and O_3 from the early measurement phase (28 Aug - 5 Sep) to the later TACTS flights (23 Sep- 26 Sep). The tracer distribution for each period is calculated in bins of equivalent latitude and potential temperature. Figure 10 shows the data coverage for each period. Figure 11 shows the mean distributions for N_2O, CO and O_3 in the early and later period and their differences. Also given is the location of the thermal and dynamical tropopause for each period as well as isolines of PV = 6 and 8 pvu.

Comparing the tracer distribution of the two phases reveals a slight increase of tropospheric tracers in the stratosphere beyond PV > 8 pvu. This region is clearly above the ExTL which extends to $\Delta\Theta = 30$ K above the local tropopause (Hoor et al., 2004, 2010). Above the ExTL with $\Delta\Theta >$ 30 K (relative to the tropopause) an increase in N_2O is observed. O_3 exhibits lower values for the same region during the final phase of the measurements. Both tracers indicate an increasing impact of tropospheric air masses in the extratropical stratosphere above the ExTL. In the tropopause region below 8 pvu the tracer signature is less clear: The distributions of both, CO and N_2O indicate a slight decrease closer to the tropopause, however with a large variability, which is even more pronounced in ozone. To further investigate, if transport from the Asian monsoon anticyclone is responsible for this increase of tropospheric tracers above the ExTL we analyzed ClaMS trajectories for the whole TACTS period. Fig. 12 shows the percentage of 50-day backward trajectories originating in the Asian monsoon region (criteria: 25°N $<$ TRA-latitude $<$ 40°N, 40°E $<$ TRA-longitude $<$ 110°E and Tra-$\Theta >$ 360 K at t = -30 days) using the same coordinate system as Fig. 11. These thresholds were chosen according to the mean location of the geopotential anomaly of the anticyclone which is shown in Fig. 13. It shows the mean location of the geopotential anomaly relative to the mean geopotential height during JJA in the monsoon area according to Bergman et al. (2013). The dark blue line indicates the monsoon location according to the threshold from Bergman et al. (2013) at 100 hPa (light blue for 200 hPa). The red contour marks the zero line for anomaly using the mean geopotential height from summer 2012 as threshold to calculate the anomaly. The difference of the monsoon contribution according to the trajectories in Fig. 12 also shows a bimodal pattern similar to the tracer observations. Trajectories originating from the Asian monsoon region affecting the ExTL are predominantly found for the initial phase of TACTS. In the lower stratosphere above the ExTL, roughly coinciding with the 8 pvu contour, trajectories indicating air masses from the Asian monsoon region are mainly found for the second phase of TACTS. The mean residence time (not shown) of these trajectories within the Asian monsoon anticyclone shows no significant difference for both regions and time periods. The trajectories provide evidence that the measured increased tropospheric influence in the extratropical lower stratosphere above the ExTL arises due to air masses from the Asian monsoon region. A decreased fraction of air masses originating from the Asian monsoon for the later measurements within ExTL indicate, in accordance to lower CO and

N_2O mixing ratios, a stronger transport barrier between the tropical troposphere and extratropical stratosphere. These results clearly indicate that the Asian monsoon has impacted the extratropical stratosphere above the ExTL during TACTS 2012.

To further analyze the tracer evolution in the LS and the ExTL we analyzed the frequency distributions of the tracers in the stratosphere for PV values exceeding PV = 8 pvu (Fig. 14). This relatively high PV value accounts for the fact that the PV at the high tropopause in the subtropics is at 5 pvu (Kunz et al., 2011). It further marks the transition from the ExTL, which is characterized by rapid transport from the local tropopause to the stratosphere (Hoor et al., 2010). For the ExTL we analyzed the PV range from 3-8 pvu (Fig. 15). The frequency distribution of selected tracers was subdivided into the different phases of TACTS. As indicated in Fig. 14 (PV $>$ 8 pvu), during the early phase (reddish colors) N_2O, CO and SF_6 are significantly lower than in the late phase. This clearly indicates an increase of tropospheric tracers accompanied with a decreasing age of air as indicated by the increase of SF_6. Ozone shows a slight decrease over time with a large variability. Water vapour and total water (CH_4 + 2 x H_2O) also show an increase over time. This finding also indicates a stronger contribution from the monsoon region which tends to moisten the mid latitude lower stratosphere during this time of the year (Randel and Jensen, 2013).

Histograms for trace gas mixing ratios in the ExTL in Fig. 15, here defined as the region between 3 and 8 pvu (Hoor et al., 2010), are less clear. The frequency distributions of CO and N_2O show a large variability and rather a stagnant or even decreasing tropospheric contribution. Reduced CO in the tropopause region indicates that the observed increase of tropospheric tracers in the lower stratosphere down to $\Theta = 350$ K (Fig. 11) is not due to isentropic transport across the subtropical jet. If rapid transport of tropospheric air into the stratosphere were responsible for the increased tropospheric signatures above the ExTL, CO would also have increased in the ExTL. Therefore the transport of relatively young stratospheric air masses with a large tropospheric air mass fraction at $\Theta > 380$ K is responsible for larger mixing ratios of tropospheric (N_2O and CO) and lower mixing ratios of stratospheric tracers (O_3) above the ExTL. At mid- and high-latitudes these air masses subsequently descend to lower potential temperatures. These results are in accordance with previous studies regarding the Ex-UTLS region (Hoor et al., 2002, 2004, 2010; Bönisch et al., 2009; Hegglin et al., 2006). It is likely that strengthening of the jet stream in September weakens transport of tropospheric air masses into the ExTL (Haynes and Shuckburgh, 2000; Berthet et al., 2007; Sawa et al., 2008), which subsequently leads to lower CO mixing ratios at the final stage of the TACTS measurements. Independent of this transport pathway, the transport of Asian monsoon influenced air masses (as measured during TACTS Fligth 2) by the shallow branch of the Brewer-Dobson-circulation above $\Theta = 400$ K leads to a stronger tropospheric influence above the ExTL.

5 Discussion and Summary

The tracer measurements over Europe during TACTS 2012 and the backward trajectory analysis provide a coherent picture, indicating a significant influence of the Asian summer monsoon on the mid-latitude UTLS. The combination of tools provide a consistent picture, which can be summarized as follows.

1. Based on in-situ trace gas measurements, irreversible mixing of different air masses in the Ex-UTLS above Θ = 380 K was observed during TACTS 2012.

2. The tropospheric endmember approximation shows that the observed irreversible mixing occured rather between stratospheric air masses with different tropospheric contributions than between undiluted tropospheric and stratospheric air masses.

3. Backward trajectories indicate that the younger of the mixed stratospheric air masses were affected by the Asian monsoon circulation.

4. An effect of the Asian monsoon on the LS over Europe is also evident from the overall trace gas distributions measured during TACTS 2012. These show that the Ex-UTLS composition over Europe has significantly changed within 20 - 30 days during the campaign. Above the ExTL a stronger impact of tropospherically influenced air masses in late September compared to late August 2012 is indicated by larger CO and N_2O, and lower O_3 mixing ratios. Within the ExTL a weakening of the tropospheric influence is indicated by decreasing CO.

5. Backward trajectories indicate that the Asian monsoon strongly affected the LS predominantely during the late phase of TACTS 2012. Within the ExTL such trajectories are preferably found during the initial phase of the campaign.

Our study suggests that the transport of air masses from the Asian monsoon region into the extratropical stratosphere is a major driver of the change of the Ex-UTLS chemical composition during summer and autumn of the northern hemisphere (Hoor et al., 2005; Hegglin and Shepherd, 2007; Bönisch et al., 2009). In-situ data of N_2O, CO and O_3 indicate a significant increase of the tropospheric impact in the extratropical lower stratosphere above the ExTL within a few weeks. This finding indicates that water vapour (Ploeger et al., 2013; Randel and Jensen, 2013) as well as other atmospheric constituents (and pollutants), which were not measured, are potentially affected by transport from the the Asian monsoon circulation.

A case study based on in-situ data shows that air masses originating from the Asian monsoon are quasi-isentropically transported above $\Theta = 380$ K into the Ex-ULTS during summer and autumn 2012. This confirms the results of model simulations and satellite data of Ploeger et al. (2013), which show an enhanced water vapour transport from the tropics (and the Asian monsoon region

into the extratropics during boreal summer above Θ = 380 K. A relatively large effective diffusivity between the tropics and extratropics during summer and autumn for potential temperatures ranging from 380 to 450 K is also in accordance with our results (Haynes and Shuckburgh, 2000).

Further, Haynes and Shuckburgh (2000) calculate a decreasing effective diffusivity from summer to autumn for Θ between 350 and 370 K (13 - 15 km), which indicates an increasing transport barrier from the early to the late monsoon season at the jet location. The measurement of lower CO within the ExTL during the later phase of TACTS compared to the initial phase agrees with a stronger transport barrier for mixing across the tropopause below Θ = 380 K. In accordance, Ploeger et al. (2015) diagnose on the basis of the PV-gradient a strong transport barrier that separates the anticyclone from its surrounding and inhibits isentropic transport and mixing between Θ = 360 - 380 K. Our measurements also support the hypothesis of an efficient transport of tropospheric trace gases (e.g. CO) to the upper Asian monsoon troposphere (Bergman et al., 2013). From the upper tropospheric monsoon region a significant fraction of these air masses is efficently transported and mixed into the lower stratosphere of mid- and high-latitudes at potential temperatures $\Theta > 380$ K (Berthet et al., 2007). Thus, our data shows that the Asian summer monsoon significantly affects the overall tracer distribution over Europe with increasing efficiency from August to September 2012.

6 Conclusions

In-situ measurements of CO, O_3 and N_2O during TACTS 2012 show a significant change of the trace gas composition over the course of four weeks in the Ex-UTLS up to Θ = 410 K. From August to late September 2012 a significant increase of N_2O and CO (and decreasing O_3) indicate a stronger tropospheric contribution above the ExTL up to Θ = 410 K. Decreasing CO mixing ratios in the ExTL below Θ = 370 K indicate a weakening of the quasi-isentropic transport across the tropopause at the jetstream into the lowermost stratosphere (Pan et al., 2006). Therefore, it is concluded that the observed increase of the tropospheric fraction above the ExTL is not caused by quasi-isentropic cross tropopause transport at the jetstream. We conclude that the observed increase in tropospheric influence in the ExTL above 370 K originates in a region with a high tropopause. The calculation of 50-day back trajectories with CLaMS-TRAJ shows that the Asian summer monsoon significantly influences the composition of the Ex-UTLS during TACTS 2012. In agreement with the tracer observations, the CLaMS trajectories show an increasing contribution of air originating in the Asian summer monsoon to the extratropical lower stratosphere during September 2012. Notably, the trajectories exhibit a mean residence time of t $>$ 200 h in the Asian monsoon anticyclone in the last 50 days before the measurements. Within the monsoon circulation the trajectories slowly rise up to $\Theta > 400$ K. As shown in a case study in Sect. 3, the monsoon affected air masses are transported to the measurement region within 30 days. For the global tracer distribution increasing SF_6 values for the late phase of the measurements consistently indicate an increasing contribution of younger

air in agreement with the analysis of the backward trajectories. Further, the simultaneously observed increase of (total) water vapour for the same air masses is in accordance with the horizontal tape recorder of H_2O at Θ = 390 K caused by the Asian monsoon (Randel and Jensen, 2013). Thus, the Asian summer monsoon significantly affected the Ex-UTLS during TACTS 2012. This indicates, that the ASM might in general significantly contribute to the flushing of the boreal extropical lower stratosphere from summer to autumn (Hegglin and Shepherd, 2007) when the tropospheric signature is at maximum (Hoor et al., 2005; Bönisch et al., 2009).

Acknowledgements. Thanks go to Michael Sprenger and Heini Wernli for the calculation of tropopause informations and providing ECMWF data. Further we thank Horst Fischer for helpful discussions and comments on the manuscript and for providing the TRIHOP instrument. Also the technical support before and during the TACTS campaign by Uwe Parchatka and Rainer Königstedt is acknowledged. Particulary we thank the flight department of the DLR, especially the pilots, for execution of the flights. We also thank the University of Mainz for financial support of the experiments. Flight planning for the TACTS/ESMVal campaign was assisted with CLaMS model forecasts, supported by the German Research Foundation (DFG) through project LASSO (HALO-SPP 1294/GR3786).

References

Assonov, S., Brenninkmeijer, C., Schuck, T., and Umezawa, T.: N_2O as a tracer of mixing stratospheric and tropospheric air based on CARIBIC data with applications for CO_2, Atmos. Environ., 79, 769–779, doi:10.1016/j.atmosenv.2013.07.035, http://linkinghub.elsevier.com/retrieve/pii/S1352231013005566, 2013.

Baker, A. K., Schuck, T. J., Slemr, F., van Velthoven, P., Zahn, A., and Brenninkmeijer, C. A. M.: Characterization of non-methane hydrocarbons in Asian summer monsoon outflow observed by the CARIBIC aircraft, Atmos. Chem. Phys., 11, 503–518, doi:10.5194/acp-11-503-2011, http://www.atmos-chem-phys.net/11/503/2011/http://www.atmos-chem-phys.net/11/503/2011/acp-11-503-2011.pdf, 2011.

Bergman, J. W., Fierli, F., Jensen, E. J., Honomichl, S., and Pan, L. L.: Boundary layer sources for the Asian anticyclone: Regional contributions to a vertical conduit, J. Geophys. Res. Atmos., 118, 2560–2575, doi:10.1002/jgrd.50142, http://dx.doi.org/10.1002/jgrd.50142, 2013.

Berthet, G., Esler, J. G., and Haynes, P. H.: A Lagrangian perspective of the tropopause and the ventilation of the lowermost stratosphere, J. Geophys. Res., 112, D18 102, doi:10.1029/2006JD008295, http://doi.wiley.com/10.1029/2006JD008295, 2007.

Birner, T. and Bönisch, H.: Residual circulation trajectories and transit times into the extratropical lowermost stratosphere, Atmos. Chem. Phys., 11, 817–827, doi:10.5194/acp-11-817-2011, http://www.atmos-chem-phys.net/11/817/2011/http://www.atmos-chem-phys.net/11/817/2011/acp-11-817-2011.pdf, 2011.

Bönisch, H., Engel, A., Curtius, J., Birner, T., and Hoor, P.: Quantifying transport into the lowermost stratosphere using simultaneous in-situ measurements of SF_6 and CO_2, Atmos. Chem. Phys., 9, 5905–5919, doi:10.5194/acp-9-5905-2009, http://www.atmos-chem-phys.net/9/5905/2009/, 2009.

Bourassa, A. E., Robock, A., Randel, W. J., Deshler, T., Rieger, L. A., Lloyd, N. D., Llewellyn, E. J., and Degenstein, D. A.: Large volcanic aerosol load in the stratosphere linked to Asian monsoon transport., Science, 337, 78–81, doi:10.1126/science.1219371, http://www.ncbi.nlm.nih.gov/pubmed/22767926, 2012.

Brewer, A. W.: Evidence for a world circulation provided by the measurements of helium and water vapour distribution in the stratosphere, Q. J. R. Meteorol. Soc., 75, 351–363, doi:10.1002/qj.49707532603, http://dx.doi.org/10.1002/qj.49707532603, 1949.

Butchart, N.: The Brewer-Dobson circulation, Rev. Geophys., 52, 157–184, doi:10.1002/2013RG000448, http://dx.doi.org/10.1002/2013RG000448, 2014.

Chen, B., Xu, X. D., Yang, S., and Zhao, T. L.: Climatological perspectives of air transport from atmospheric boundary layer to tropopause layer over Asian monsoon regions during boreal summer inferred from Lagrangian approach, Atmos. Chem. Phys., 12, 5827–5839, doi:10.5194/acp-12-5827-2012, http://www.atmos-chem-phys.net/12/5827/2012/http://www.atmos-chem-phys.net/12/5827/2012/acp-12-5827-2012.pdf, 2012.

Dee, D. P., Uppala, S. M., Simmons, A. J., Berrisford, P., Poli, P., Kobayashi, S., Andrae, U., Balmaseda, M. A., Balsamo, G., Bauer, P., Bechtold, P., Beljaars, A. C. M., van de Berg, L., Bidlot, J., Bormann, N., Delsol, C., Dragani, R., Fuentes, M., Geer, A. J., Haimberger, L., Healy, S. B., Hersbach, H., Hólm, E. V., Isaksen, L., Kållberg, P., Köhler, M., Matricardi, M., McNally, A. P., Monge-Sanz, B. M., Morcrette, J.-J., Park, B.-K., Peubey, C., de Rosnay, P., Tavolato, C., Thépaut, J.-N., and Vitart, F.: The ERA-Interim

reanalysis: configuration and performance of the data assimilation system, Q. J. R. Meteorol. Soc., 137, 553–597, doi:10.1002/qj.828, http://dx.doi.org/10.1002/qj.828, 2011.

Dobson, G. M. B.: Origin and Distribution of the Polyatomic Molecules in the Atmosphere, Proc. R. Soc. London. Ser. A. Math. Phys. Sci., 236, 187–193, http://rspa.royalsocietypublishing.org/content/236/1205/187.short, 1956.

Fadnavis, S., Semeniuk, K., Pozzoli, L., Schultz, M. G., Ghude, S. D., Das, S., and Kakatkar, R.: Transport of aerosols into the UTLS and their impact on the Asian monsoon region as seen in a global model simulation, Atmos. Chem. Phys., 13, 8771–8786, doi:10.5194/acp-13-8771-2013, http://www.atmos-chem-phys.net/13/8771/2013/http://www.atmos-chem-phys.net/13/8771/2013/acp-13-8771-2013.pdf, 2013.

Fadnavis, S., Schultz, M. G., Semeniuk, K., Mahajan, A. S., Pozzoli, L., Sonbawne, S., Ghude, S. D., Kiefer, M., and Eckert, E.: Trends in peroxyacetyl nitrate (PAN) in the upper troposphere and lower stratosphere over southern Asia during the summer monsoon season: regional impacts, Atmos. Chem. Phys., 14, 12 725–12 743, doi:10.5194/acp-14-12725-2014, http://www.atmos-chem-phys.net/14/12725/2014/http://www.atmos-chem-phys.net/14/12725/2014/acp-14-12725-2014.pdf, 2014.

Fadnavis, S., Semeniuk, K., Schultz, M. G., Kiefer, M., Mahajan, A., Pozzoli, L., and Sonbawane, S.: Transport pathways of peroxyacetyl nitrate in the upper troposphere and lower stratosphere from different monsoon systems during the summer monsoon season, Atmos. Chem. Phys., 15, 11 477–11 499, doi:10.5194/acp-15-11477-2015, http://www.atmos-chem-phys.net/15/11477/2015/http://www.atmos-chem-phys.net/15/11477/2015/acp-15-11477-2015.pdf, 2015.

Fischer, H., Wienhold, F. G., Hoor, P., Bujok, O., Schiller, C., Siegmund, P., Ambaum, M., Scheeren, H. A., and Lelieveld, J.: Tracer correlations in the northern high latitude lowermost stratosphere: Influence of cross-tropopause mass exchange, Geophys. Res. Lett., 27, 97–100, doi:10.1029/1999GL010879, http://doi.wiley.com/10.1029/1999GL010879, 2000.

Flocke, F., Herman, R. L., Salawitch, R. J., Atlas, E., Webster, C. R., Schauffler, S. M., Lueb, R. A., May, R. D., Moyer, E. J., Rosenlof, K. H., Scott, D. C., Blake, D. R., and Bui, T. P.: An examination of chemistry and transport processes in the tropical lower stratosphere using observations of long-lived and short-lived compounds obtained during STRAT and POLARIS, J. Geophys. Res. Atmos., 104, 26 625–26 642, doi:10.1029/1999JD900504, http://dx.doi.org/10.1029/1999JD900504, 1999.

Forster, P. M. d. F. and Shine, K. P.: Assessing the climate impact of trends in stratospheric water vapor, Geophys. Res. Lett., 29, 10–14, doi:10.1029/2001GL013909, http://dx.doi.org/10.1029/2001GL013909, 2002.

Fueglistaler, S., Dessler, A. E., Dunkerton, T. J., Folkins, I., Fu, Q., and Mote, P. W.: Tropical tropopause layer, Rev. Geophys., 47, RG1004, doi:10.1029/2008RG000267, http://dx.doi.org/10.1029/2008RG000267, 2009.

Garny, H. and Randel, W. J.: Dynamic variability of the Asian monsoon anticyclone observed in potential vorticity and correlations with tracer distributions, J. Geophys. Res. Atmos., 118, 13,413–421,433, doi:10.1002/2013JD020908, http://dx.doi.org/10.1002/2013JD020908, 2013.

Garny, H. and Randel, W. J.: Transport pathways from the Asian monsoon anticyclone to the stratosphere, Atmos. Chem. Phys. Discuss., 15, 25 981–26 023, doi:10.5194/acpd-15-25981-2015, http://www.atmos-chem-phys-discuss.net/15/25981/2015/http://www.atmos-chem-phys-discuss.net/15/25981/2015/acpd-15-25981-2015.pdf, 2015.

Gettelman, A., Hoor, P., Pan, L. L., Randel, W. J., Hegglin, M. I., and Birner, T.: The extratropical upper troposphere and lower stratosphere, Rev. Geophys., 49, RG3003, doi:10.1029/2011RG000355, http://dx.doi.org/10.1029/2011RG000355, 2011.

Glatthor, N., von Clarmann, T., Stiller, G. P., Funke, B., Koukouli, M. E., Fischer, H., Grabowski, U., Höpfner, M., Kellmann, S., and Linden, A.: Large-scale upper tropospheric pollution observed by MIPAS HCN and C₂H₆ global distributions, Atmos. Chem. Phys., 9, 9619–9634, doi:10.5194/acp-9-9619-2009, http://www.atmos-chem-phys.net/9/9619/2009/http://www.atmos-chem-phys.net/9/9619/2009/acp-9-9619-2009.pdf, 2009.

Haynes, P. and Shuckburgh, E.: Effective diffusivity as a diagnostic of atmospheric transport: 2. Troposphere and lower stratosphere, J. Geophys. Res. Atmos., 105, 22 795–22 810, doi:10.1029/2000JD900092, http://dx.doi.org/10.1029/2000JD900092, 2000.

Hegglin, M. I. and Shepherd, T. G.: O_3-N_2O correlations from the Atmospheric Chemistry Experiment: Revisiting a diagnostic of transport and chemistry in the stratosphere, J. Geophys. Res., 112, D19 301, doi:10.1029/2006JD008281, http://doi.wiley.com/10.1029/2006JD008281, 2007.

Hegglin, M. I. and Shepherd, T. G.: Large climate-induced changes in ultraviolet index and stratosphere-to-troposphere ozone flux, Nat. Geosci, 2, 687–691, http://dx.doi.org/10.1038/ngeo604http://www.nature.com/ngeo/journal/v2/n10/suppinfo/ngeo604_S1.html, 2009.

Hegglin, M. I., Brunner, D., Peter, T., Hoor, P., Fischer, H., Staehelin, J., Krebsbach, M., Schiller, C., Parchatka, U., and Weers, U.: Measurements of NO, NO_y, N_2O, and O_3 during SPURT: implications for transport and chemistry in the lowermost stratosphere, Atmos. Chem. Phys., 6, 1331–1350, doi:10.5194/acp-6-1331-2006, http://www.atmos-chem-phys.net/6/1331/2006/http://www.atmos-chem-phys.net/6/1331/2006/acp-6-1331-2006.pdf, 2006.

Herman, R. L., Webster, C. R., May, R. D., Scott, D. C., Hu, H., Moyer, E. J., Wennberg, P. O., Hanisco, T. F., Lanzendorf, E. J., Salawitch, R. J., Yung, Y. L., Margitan, J. J., and Bui, T. P.: Measurements of CO in the upper troposphere and lower stratosphere, Chemosph. - Glob. Chang. Sci., 1, 173–183, doi:http://dx.doi.org/10.1016/S1465-9972(99)00008-2, http://www.sciencedirect.com/science/article/pii/S1465997299000082, 1999.

Highwood, E. J. and Hoskins, B. J.: The tropical tropopause, Q. J. R. Meteorol. Soc., 124, 1579–1604, doi:10.1002/qj.49712454911, http://dx.doi.org/10.1002/qj.49712454911, 1998.

Hintsa, E. J., Boering, K. A., Weinstock, E. M., Anderson, J. G., Gary, B. L., Pfister, L., Daube, B. C., Wofsy, S. C., Loewenstein, M., Podolske, J. R., Margitan, J. J., and Bui, T. P.: Troposphere-to-stratosphere transport in the lowermost stratosphere from measurements of H2O, CO2, N2O and O3, Geophys. Res. Lett., 25, 2655–2658, doi:10.1029/98GL01797, http://dx.doi.org/10.1029/98GL01797, 1998.

Holton, J. R., Haynes, P. H., McIntyre, M. E., Douglass, A. R., Rood, R. B., and Pfister, L.: Stratosphere-troposphere exchange, Rev. Geophys., 33, 403–439, doi:10.1029/95RG02097, http://dx.doi.org/10.1029/95RG02097, 1995.

Hoor, P., Fischer, H., Lange, L., Lelieveld, J., and Brunner, D.: Seasonal variations of a mixing layer in the lowermost stratosphere as identified by the CO-O_3 correlation from in situ measurements, J. Geophys. Res. Atmos., 107, ACL 1–1–ACL 1–11, doi:10.1029/2000JD000289, http://dx.doi.org/10.1029/2000JD000289, 2002.

Hoor, P., Gurk, C., Brunner, D., Hegglin, M. I., Wernli, H., and Fischer, H.: Seasonality and extent of extratropical TST derived from in-situ CO measurements during SPURT, Atmos. Chem. Phys., 4, 1427–1442, doi:10.5194/acp-4-1427-2004, http://www.atmos-chem-phys.net/4/1427/2004/http://www.atmos-chem-phys.net/4/1427/2004/acp-4-1427-2004.pdf, 2004.

Hoor, P., Fischer, H., and Lelieveld, J.: Tropical and extratropical tropospheric air in the lowermost stratosphere over Europe: A CO-based budget, Geophys. Res. Lett., 32, L07 802, doi:10.1029/2004GL022018, http://dx.doi.org/10.1029/2004GL022018, 2005.

Hoor, P., Wernli, H., Hegglin, M. I., and Bönisch, H.: Transport timescales and tracer properties in the extratropical UTLS, Atmos. Chem. Phys., 10, 7929–7944, doi:10.5194/acp-10-7929-2010, http://www.atmos-chem-phys.net/10/7929/2010/, 2010.

Hoskins, B. J., McIntyre, M. E., and Robertson, A. W.: On the use and significance of isentropic potential vorticity maps, Q. J. R. Meteorol. Soc., 111, 877–946, doi:10.1002/qj.49711147002, http://dx.doi.org/10.1002/qj.49711147002, 1985.

Hsu, C. J. and Plumb, R. A.: Nonaxisymmetric Thermally Driven Circulations and Upper-Tropospheric Monsoon Dynamics, J. Atmos. Sci., 57, 1255–1276, doi:10.1175/1520-0469(2000)057<1255:NTDCAU>2.0.CO;2, http://dx.doi.org/10.1175/1520-0469(2000)057<1255:NTDCAU>2.0.CO2, 2000.

James, R. and Legras, B.: Mixing processes and exchanges in the tropical and the subtropical UT/LS, Atmos. Chem. Phys., 9, 25–38, doi:10.5194/acp-9-25-2009, http://www.atmos-chem-phys.net/9/25/2009/http://www.atmos-chem-phys.net/9/25/2009/acp-9-25-2009.pdf, 2009.

Jurkat, T., Voigt, C., Kaufmann, S., Zahn, A., Sprenger, M., Hoor, P., Bozem, H., Müller, S., Dörnbrack, A., Schlager, H., Bönisch, H., and Engel, A.: A quantitative analysis of stratospheric HCl, HNO_3, and O_3 in the tropopause region near the subtropical jet, Geophys. Res. Lett., 41, 3315–3321, doi:10.1002/2013GL059159, http://dx.doi.org/10.1002/2013GL059159, 2014.

Konopka, P. and Pan, L. L.: On the mixing-driven formation of the Extratropical Transition Layer (ExTL), J. Geophys. Res. Atmos., 117, D18 301, doi:10.1029/2012JD017876, http://dx.doi.org/10.1029/2012JD017876, 2012.

Konopka, P., Grooß, J.-U., Günther, G., Ploeger, F., Pommrich, R., Müller, R., and Livesey, N.: Annual cycle of ozone at and above the tropical tropopause: observations versus simulations with the Chemical Lagrangian Model of the Stratosphere (CLaMS), Atmos. Chem. Phys., 10, 121–132, doi:10.5194/acp-10-121-2010, http://www.atmos-chem-phys.net/10/121/2010/http://www.atmos-chem-phys.net/10/121/2010/acp-10-121-2010.pdf, 2010.

Kumar, A., Wu, S., Weise, M. F., Honrath, R., Owen, R. C., Helmig, D., Kramer, L., Val Martin, M., and Li, Q.: Free-troposphere ozone and carbon monoxide over the North Atlantic for 2001–2011, Atmos. Chem. Phys., 13, 12 537–12 547, doi:10.5194/acp-13-12537-2013, http://www.atmos-chem-phys.net/13/12537/2013/http://www.atmos-chem-phys.net/13/12537/2013/acp-13-12537-2013.pdf, 2013.

Kunz, A., Konopka, P., Müller, R., and Pan, L. L.: Dynamical tropopause based on isentropic potential vorticity gradients, J. Geophys. Res., 116, D01 110, doi:10.1029/2010JD014343, http://doi.wiley.com/10.1029/2010JD014343, 2011.

McKenna, D. S., Grooß, J.-U., Günther, G., Konopka, P., Müller, R., Carver, G., and Sasano, Y.: A new Chemical Lagrangian Model of the Stratosphere (CLaMS) 2. Formulation of chemistry scheme and initialization, J. Geophys. Res. Atmos., 107, ACH 4–1–ACH 4–14, doi:10.1029/2000JD000113, http://dx.doi.org/10.1029/2000JD000113, 2002a.

McKenna, D. S., Konopka, P., Grooß, J.-U., Günther, G., Müller, R., Spang, R., Offermann, D., and Orsolini, Y.: A new Chemical Lagrangian Model of the Stratosphere (CLaMS) 1. Formulation of advection and mixing, J. Geophys. Res. Atmos., 107, ACH 15–1–ACH 15–15, doi:10.1029/2000JD000114, http://dx.doi.org/10.1029/2000JD000114, 2002b.

Müller, S., Hoor, P., Berkes, F., Bozem, H., Klingebiel, M., Reutter, P., Smit, H. G. J., Wendisch, M., Spichtinger, P., and Borrmann, S.: In situ detection of stratosphere-troposphere exchange of cirrus particles in the midlatitudes, Geophys. Res. Lett., 42, 949–955, doi:10.1002/2014GL062556, http://dx.doi.org/10.1002/2014GL062556, 2015.

Palazzi, E., Fierli, F., Cairo, F., Cagnazzo, C., Di Donfrancesco, G., Manzini, E., Ravegnani, F., Schiller, C., D'Amato, F., and Volk, C. M.: Diagnostics of the Tropical Tropopause Layer from in-situ observations and CCM data, Atmos. Chem. Phys., 9, 9349–9367, doi:10.5194/acp-9-9349-2009, http://www.atmos-chem-phys.net/9/9349/2009/, 2009.

Pan, L. L.: Definitions and sharpness of the extratropical tropopause: A trace gas perspective, J. Geophys. Res., 109, D23 103, doi:10.1029/2004JD004982, http://doi.wiley.com/10.1029/2004JD004982, 2004.

Pan, L. L., Konopka, P., and Browell, E. V.: Observations and model simulations of mixing near the extratropical tropopause, J. Geophys. Res., 111, D05 106, doi:10.1029/2005JD006480, http://doi.wiley.com/10.1029/2005JD006480, 2006.

Park, M., Randel, W. J., Kinnison, D. E., Garcia, R. R., and Choi, W.: Seasonal variation of methane, water vapor, and nitrogen oxides near the tropopause: Satellite observations and model simulations, J. Geophys. Res. Atmos., 109, D03 302, doi:10.1029/2003JD003706, http://dx.doi.org/10.1029/2003JD003706, 2004.

Park, M., Randel, W. J., Gettelman, A., Massie, S. T., and Jiang, J. H.: Transport above the Asian summer monsoon anticyclone inferred from Aura Microwave Limb Sounder tracers, J. Geophys. Res., 112, D16 309, doi:10.1029/2006JD008294, http://doi.wiley.com/10.1029/2006JD008294, 2007.

Park, M., Randel, W. J., Emmons, L. K., Bernath, P. F., Walker, K. a., and Boone, C. D.: Chemical isolation in the Asian monsoon anticyclone observed in Atmospheric Chemistry Experiment (ACE-FTS) data, Atmos. Chem. Phys., 8, 757–764, doi:10.5194/acp-8-757-2008, http://www.atmos-chem-phys.net/8/757/2008/, 2008.

Park, M., Randel, W. J., Emmons, L. K., and Livesey, N. J.: Transport pathways of carbon monoxide in the Asian summer monsoon diagnosed from Model of Ozone and Related Tracers (MOZART), J. Geophys. Res. Atmos., 114, D08 303, doi:10.1029/2008JD010621, http://dx.doi.org/10.1029/2008JD010621, 2009.

Ploeger, F., Konopka, P., Günther, G., Grooß, J.-U., and Müller, R.: Impact of the vertical velocity scheme on modeling transport in the tropical tropopause layer, J. Geophys. Res., 115, D03 301, doi:10.1029/2009JD012023, http://doi.wiley.com/10.1029/2009JD012023, 2010.

Ploeger, F., Günther, G., Konopka, P., Fueglistaler, S., Müller, R., Hoppe, C., Kunz, A., Spang, R., Grooß, J.-U., and Riese, M.: Horizontal water vapor transport in the lower stratosphere from subtropics to high

latitudes during boreal summer, J. Geophys. Res. Atmos., 118, 8111–8127, doi:10.1002/jgrd.50636, http://dx.doi.org/10.1002/jgrd.50636, 2013.

Ploeger, F., Gottschling, C., Griessbach, S., Grooß, J.-U., Guenther, G., Konopka, P., Müller, R., Riese, M., Stroh, F., Tao, M., Ungermann, J., Vogel, B., and von Hobe, M.: A potential vorticity-based determination of the transport barrier in the Asian summer monsoon anticyclone, Atmos. Chem. Phys., 15, 13 145–13 159, doi:10.5194/acp-15-13145-2015, http://www.atmos-chem-phys.net/15/13145/2015/http://www.atmos-chem-phys.net/15/13145/2015/acp-15-13145-2015.pdf, 2015.

Pommrich, R., Müller, R., Grooß, J.-U., Konopka, P., Ploeger, F., Vogel, B., Tao, M., Hoppe, C. M., Günther, G., Spelten, N., Hoffmann, L., Pumphrey, H.-C., Viciani, S., D'Amato, F., Volk, C. M., Hoor, P., Schlager, H., and Riese, M.: Tropical troposphere to stratosphere transport of carbon monoxide and long-lived trace species in the Chemical Lagrangian Model of the Stratosphere (CLaMS), Geosci. Model Dev., 7, 2895–2916, doi:10.5194/gmd-7-2895-2014, http://www.geosci-model-dev.net/7/2895/2014/http://www.geosci-model-dev.net/7/2895/2014/gmd-7-2895-2014.pdf, 2014.

Popovic, J. M. and Plumb, R. A.: Eddy Shedding from the Upper-Tropospheric Asian Monsoon Anticyclone, J. Atmos. Sci., 58, 93–104, doi:10.1175/1520-0469(2001)058<0093:ESFTUT>2.0.CO;2, http://dx.doi.org/10.1175/1520-0469(2001)058<0093:ESFTUT>2.0.CO2, 2001.

Press, W., Teukolsky, S., Vetterling, W., Flannery, B., and Yudin, V.: Numerical Recipes: The Art of Scientific Computing, Cambridge Univ. Press Cambridge, New York, 2nd edn., 1992.

Randel, W. J. and Jensen, E. J.: Physical processes in the tropical tropopause layer and their roles in a changing climate, Nat. Geosci, 6, 169–176, http://dx.doi.org/10.1038/ngeo1733, 2013.

Randel, W. J. and Park, M.: Deep convective influence on the Asian summer monsoon anticyclone and associated tracer variability observed with Atmospheric Infrared Sounder (AIRS), J. Geophys. Res. Atmos., 111, D12 314, doi:10.1029/2005JD006490, http://dx.doi.org/10.1029/2005JD006490, 2006.

Randel, W. J., Seidel, D. J., and Pan, L. L.: Observational characteristics of double tropopauses, J. Geophys. Res., 112, D07 309, doi:10.1029/2006JD007904, http://doi.wiley.com/10.1029/2006JD007904, 2007.

Randel, W. J., Park, M., Emmons, L., Kinnison, D., Bernath, P., Walker, K. A., Boone, C., and Pumphrey, H.: Asian monsoon transport of pollution to the stratosphere., Science, 328, 611–3, doi:10.1126/science.1182274, http://www.ncbi.nlm.nih.gov/pubmed/20339030, 2010.

Richter, A., Burrows, J. P., Nusz, H., Granier, C., and Niemeier, U.: Increase in tropospheric nitrogen dioxide over China observed from space, Nature, 437, 129–132, http://dx.doi.org/10.1038/nature04092http://www.nature.com/nature/journal/v437/n7055/suppinfo/nature04092_S1.html, 2005.

Riese, M., Ploeger, F., Rap, A., Vogel, B., Konopka, P., Dameris, M., and Forster, P.: Impact of uncertainties in atmospheric mixing on simulated UTLS composition and related radiative effects, J. Geophys. Res., 117, D16 305, doi:10.1029/2012JD017751, http://doi.wiley.com/10.1029/2012JD017751, 2012.

Riese, M., Oelhaf, H., Preusse, P., Blank, J., Ern, M., Friedl-Vallon, F., Fischer, H., Guggenmoser, T., Höpfner, M., Hoor, P., Kaufmann, M., Orphal, J., Plöger, F., Spang, R., Suminska-Ebersoldt, O., Ungermann, J., Vogel, B., and Woiwode, W.: Gimballed Limb Observer for Radiance Imaging of the Atmosphere (GLORIA) scientific objectives, Atmos. Meas. Tech., 7, 1915–1928, doi:10.5194/amt-7-1915-2014, http://www.atmos-meas-tech.net/7/1915/2014/http://www.atmos-meas-tech.net/7/1915/2014/amt-7-1915-2014.pdf, 2014.

Rosenlof, K. H., Tuck, A. F., Kelly, K. K., Russell, J. M., and McCormick, M. P.: Hemispheric asymmetries in water vapor and inferences about transport in the lower stratosphere, J. Geophys. Res. Atmos., 102, 13 213–13 234, doi:10.1029/97JD00873, http://dx.doi.org/10.1029/97JD00873, 1997.

Sawa, Y., Machida, T., and Matsueda, H.: Seasonal variations of CO2 near the tropopause observed by commercial aircraft, J. Geophys. Res. Atmos., 113, D23 301, doi:10.1029/2008JD010568, http://dx.doi.org/10.1029/2008JD010568, 2008.

Schiller, C. L., Bozem, H., Gurk, C., Parchatka, U., Königstedt, R., Harris, G. W., Lelieveld, J., and Fischer, H.: Applications of quantum cascade lasers for sensitive trace gas measurements of CO, CH_4, N_2O and HCHO, Appl. Phys. B, 92, 419–430, doi:10.1007/s00340-008-3125-0, http://dx.doi.org/10.1007/s00340-008-3125-0, 2008.

Schuck, T. J., Brenninkmeijer, C. A. M., Baker, A. K., Slemr, F., von Velthoven, P. F. J., and Zahn, A.: Greenhouse gas relationships in the Indian summer monsoon plume measured by the CARIBIC passenger aircraft, Atmos. Chem. Phys., 10, 3965–3984, doi:10.5194/acp-10-3965-2010, http://www.atmos-chem-phys.net/10/3965/2010/http://www.atmos-chem-phys.net/10/3965/2010/acp-10-3965-2010.pdf, 2010.

Spackman, J. R., Weinstock, E. M., Anderson, J. G., Hurst, D. F., Jost, H.-J., and Schauffler, S. M.: Aircraft observations of rapid meridional transport from the tropical tropopause layer into the lowermost stratosphere: Implications for midlatitude ozone, J. Geophys. Res. Atmos., 112, D12 308, doi:10.1029/2006JD007618, http://dx.doi.org/10.1029/2006JD007618, 2007.

Strahan, S. E.: Climatologies of lower stratospheric NO y and O 3 and correlations with N 2 O based on in situ observations, J. Geophys. Res., 104, 30 463, doi:10.1029/1999JD900775, http://doi.wiley.com/10.1029/1999JD900775, 1999.

Thouret, V., Cammas, J.-P., Sauvage, B., Athier, G., Zbinden, R., Nédélec, P., Simon, P., and Karcher, F.: Tropopause referenced ozone climatology and inter-annual variability (1994–2003) from the MOZAIC programme, Atmos. Chem. Phys., 6, 1033–1051, doi:10.5194/acp-6-1033-2006, http://www.atmos-chem-phys.net/6/1033/2006/, 2006.

Vogel, B., Günther, G., Müller, R., Grooß, J.-U., Hoor, P., Krämer, M., Müller, S., Zahn, A., and Riese, M.: Fast transport from Southeast Asia boundary layer sources to northern Europe: rapid uplift in typhoons and eastward eddy shedding of the Asian monsoon anticyclone, Atmos. Chem. Phys., 14, 12 745–12 762, doi:10.5194/acp-14-12745-2014, http://www.atmos-chem-phys.net/14/12745/2014/http://www.atmos-chem-phys.net/14/12745/2014/acp-14-12745-2014.pdf, 2014.

Volk, C. M., Elkins, J. W., Fahey, D. W., Salawitch, R. J., Dutton, G. S., Gilligan, J. M., Proffitt, M. H., Loewenstein, M., Podolske, J. R., Minschwaner, K., Margitan, J. J., and Chan, K. R.: Quantifying Transport Between the Tropical and Mid-Latitude Lower Stratosphere, Science (80-.)., 272, 1763–1768, http://science.sciencemag.org/content/272/5269/1763.abstract, 1996.

WMO: Meteorology - A three-dimensional science, WMO Bull., pp. 134–138, 1957.

Zahn, A. and Brenninkmeijer, C. A. M.: New Directions: A Chemical Tropopause Defined, Atmos. Environ., 37, 439–440, 2003.

Zahn, A., Brenninkmeijer, C. A. M., Maiss, M., Scharffe, D. H., Crutzen, P. J., Hermann, M., Heintzenberg, J., Wiedensohler, A., Güsten, H., Heinrich, G., Fischer, H., Cuijpers, J. W. M., and van Velthoven, P. F. J.: Identification of extratropical two-way troposphere-stratosphere mixing based on CARIBIC measurements

of O_3, CO, and ultrafine particles, J. Geophys. Res. Atmos., 105, 1527–1535, doi:10.1029/1999JD900759, http://dx.doi.org/10.1029/1999JD900759, 2000.

Zahn, A., Weppner, J., Widmann, H., Schlote-Holubek, K., Burger, B., Kühner, T., and Franke, H.: A fast and precise chemiluminescence ozone detector for eddy flux and airborne application, Atmos. Meas. Tech., 5, 363–375, doi:10.5194/amt-5-363-2012, http://www.atmos-meas-tech.net/5/363/2012/http://www.atmos-meas-tech.net/5/363/2012/amt-5-363-2012.pdf, 2012.

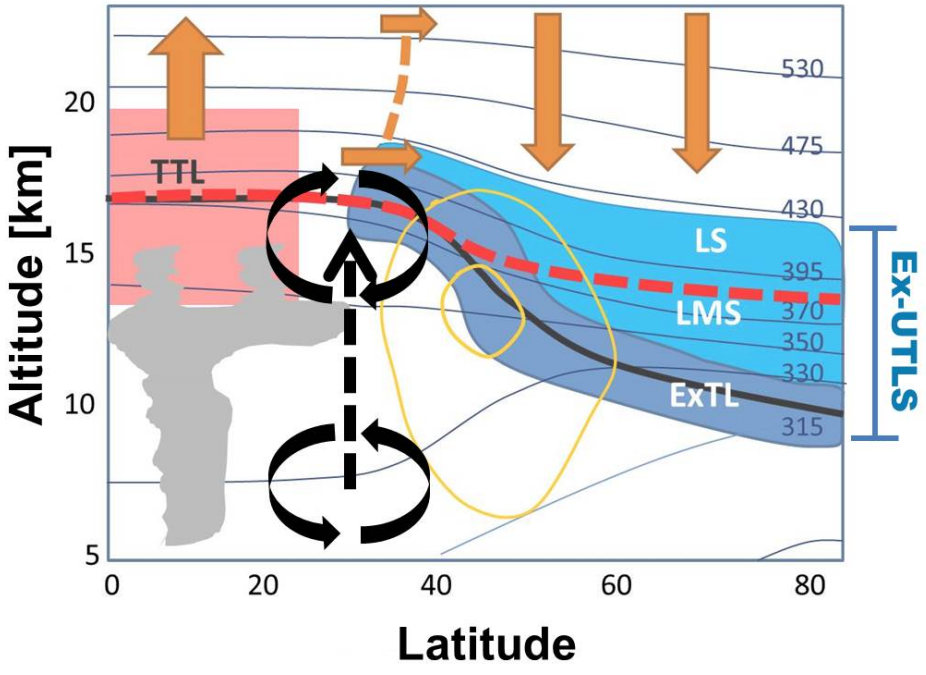

Figure 1. Illustration of the dynamical structure of the UTLS for the Northern hemispheric summer adapted from Fig. 2b of Gettelman et al. (2011) and Fig. 9 of Riese et al. (2014). The thick black line denotes the location of the thermal tropopause. Thin black lines are isentropes,the red dashed line highlights the 380 K isentrope. The location of the TTL is represented in light red. The Ex-UTLS is divided into the extratropical tropopause layer (ExTL) in dark blue and the lowermost (LMS) and lower stratosphere (LS) in light blue. The LMS and LS are vertically seperated by the 380 K isentrope. Yellow lines indicate the location of the jetstream. Orange arrows sketch the upwards transport of air masses within the TTL and descending air masses in the extratropical stratosphere. Both regions are linked by the deep (upper horizontal arrow) and shallow (lower horizontal arrow) within the stratosphere. The dashed orange line sketches the edge of the tropical pipe, which suppresses exchange between the tropical and extratropical stratosphere. The location of the Asian monsoon circulation is schematically shown in dark black.

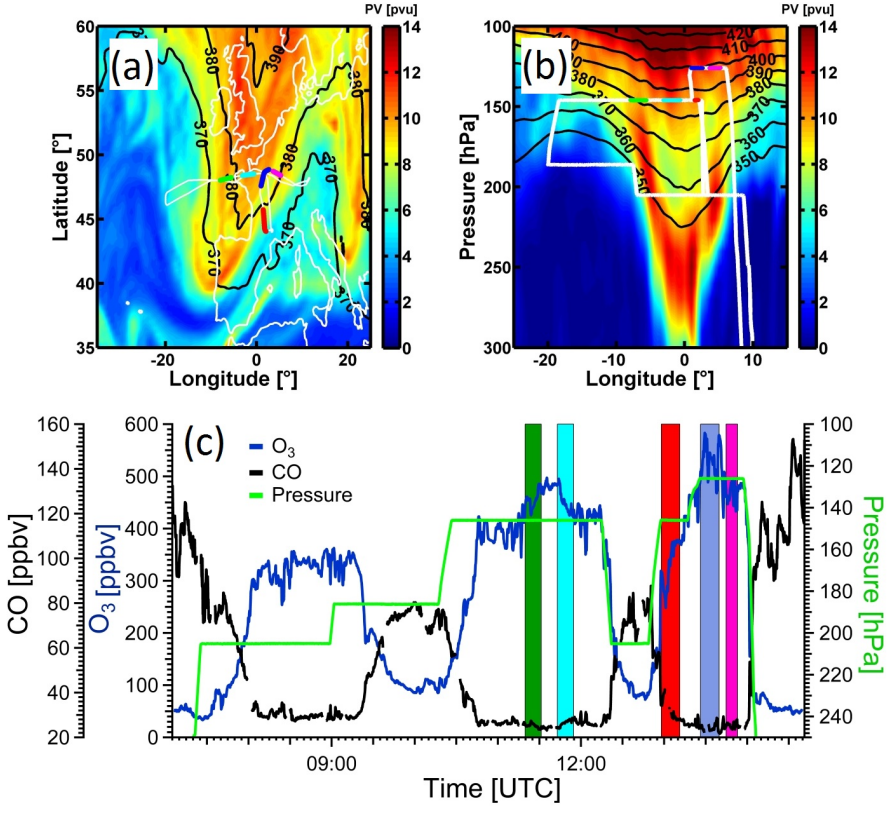

Figure 2. TACTS Flight 2 on 30 August 2012: (a) ECMWF data (15 UTC) at 150 hPa of potential vorticity (color) and potential temperature (black contour lines). The thick white line is the flight path of TACTS Flight 2. (b) Horizontal cross section of ECMWF potential vorticity data along 48.5°N. Different colors in (a) and (b) indicate flight legs with measured mixing lines (see Sec. 3). (c) Time series of CO (black), O_3 (blue) and Pressure (green). Data points which form mixing lines are colored according to panel (a) and (b). The total uncertainty of CO and O_3 is mostly within the line thickness and therefore not shown (for individual error bars see Fig. 3 and Fig.4).

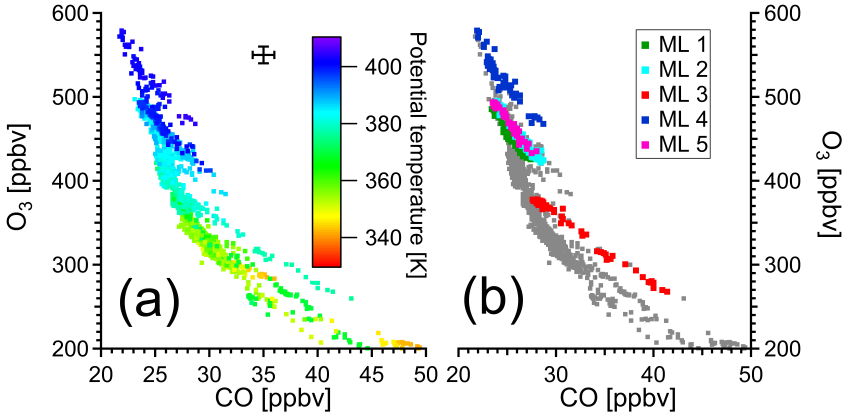

Figure 3. Stratospheric part of the CO-O_3-correlation for TACTS flight 2 on 30 August 2012: (a) Color-coded with measured potential temperature. (b) Mixing lines (ML) in different colors in accordance with Fig. 2. Uncertainties of the CO and O3 data are separately shown as a black cross.

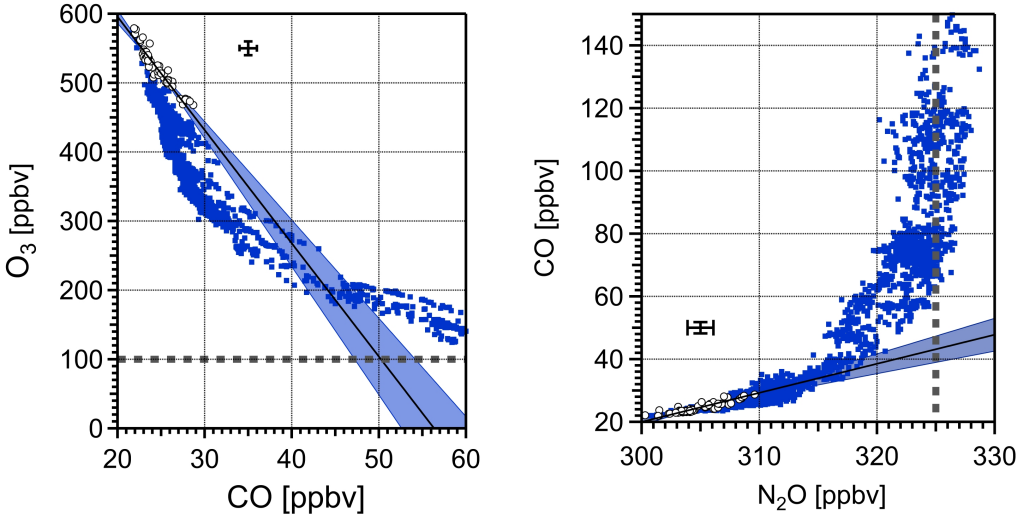

Figure 4. Linear fitting for ML 4 based on the FITEXY-routine described in Press et al. (1992). Blue dots: Scatter plot of CO and O_3 (left), and N_2O and CO (right), respectively. White dots: Data points of ML 4 on the respective scatter plot. Solid black line: Linear fit with confidence region (shaded area). Dotted lines: Assumption of a tropospheric endmember of $R(O_3)_{Trop}$ = 100 ppbv (top) and $R(N_2O)_{Trop}$ = 325 ppbv (bottom). Uncertainties are separately shown as black crosses.

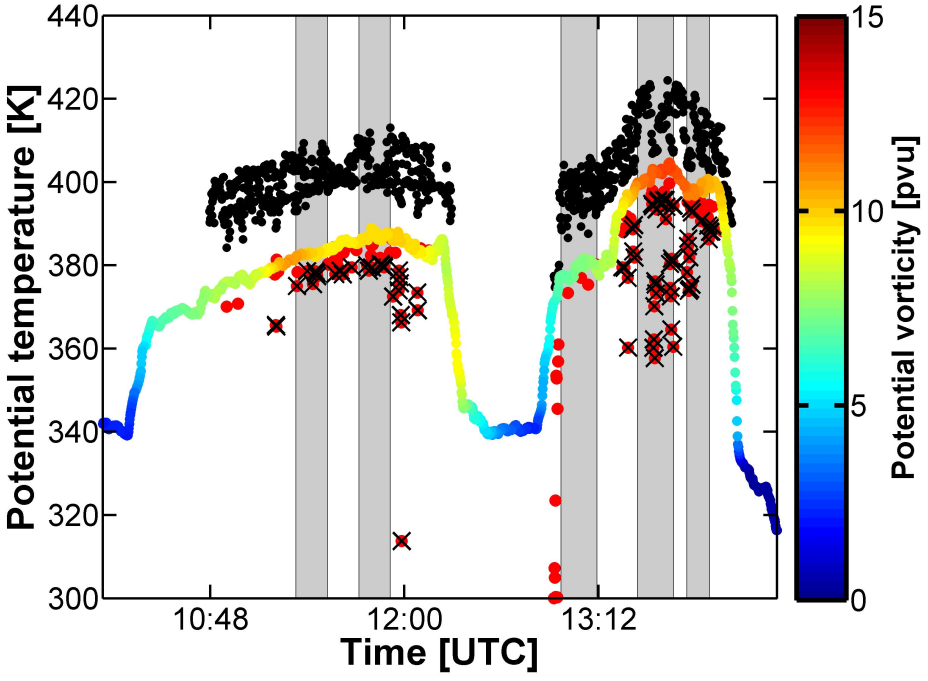

Figure 5. Solid line: Time series of the measured potential temperature Θ for the second half of TACTS Flight 2 with PV as color (from ECMWF data). Black dots: Maximum potential temperature along 50-day back trajectories for all data points with $\Theta > 370$ and PV > 4 pvu at the measurement location. Red dots: Minimum potential temperature along 50-day back trajectories for all data points with $\Theta > 370$ K, PV > 4 pvu, and minimum Θ along the backwards trajectories is smaller as Θ at the measurement. Red dots with PV > 7.5 pvu and minimum Θ at least 5 K smaller as Θ at the measurement are marked with a black cross (cf. Fig. 6).

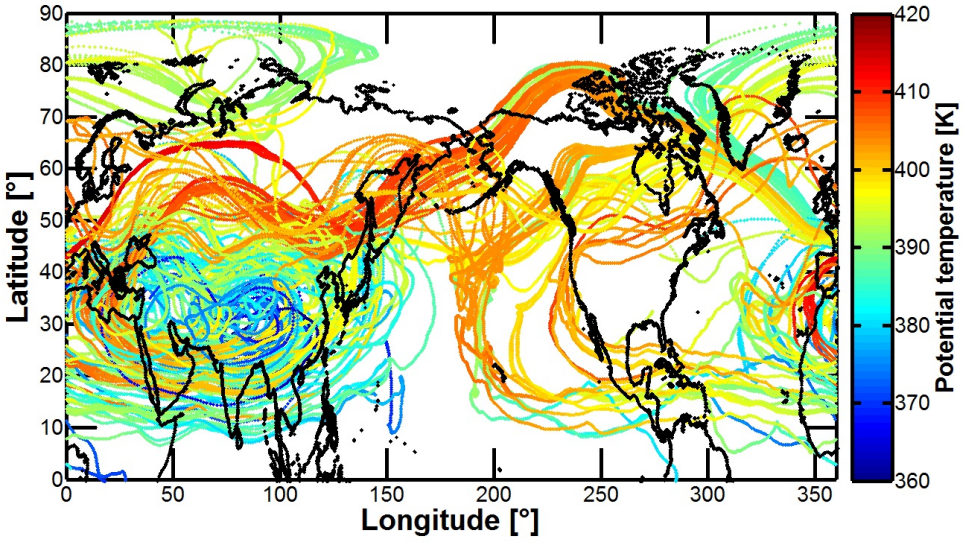

Figure 6. 50 day backward trajectories for all data points with $\Theta > 370$ K, PV > 7.5 pvu, and minimum Θ along the backwards trajectories is at least 5 K smaller as Θ at the measurement (cf. Fig. 5). Color: Potential temperature along the backward trajectories based on ERA-Interim reanalysis data.

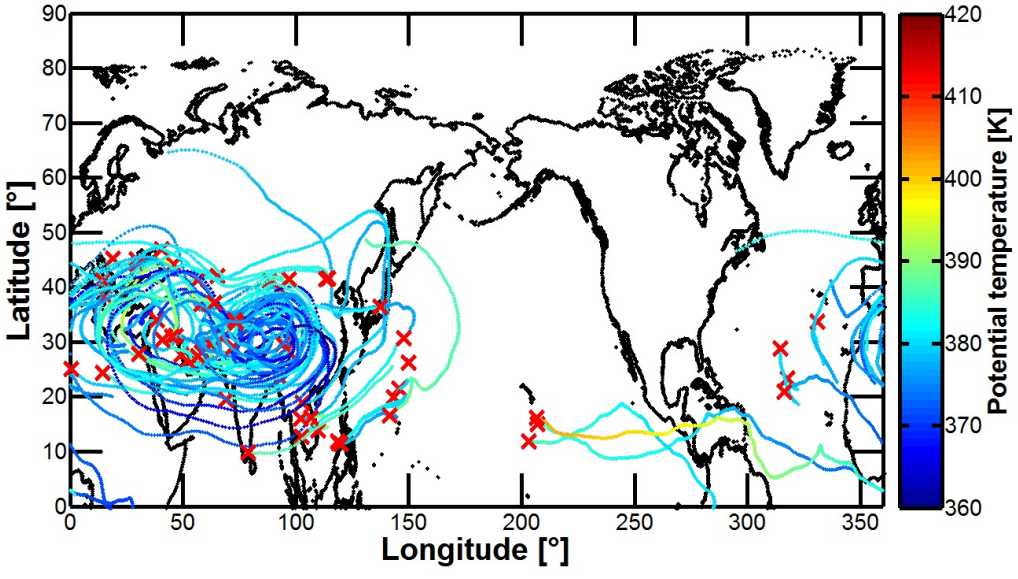

Figure 7. Pathway of the trajectory ensemble as shown in Fig. 6 with $\mathrm{PV}_{Tra} < 5$ pvu. Red crosses mark the location of the trajectories where PV values exceed 5 pvu.

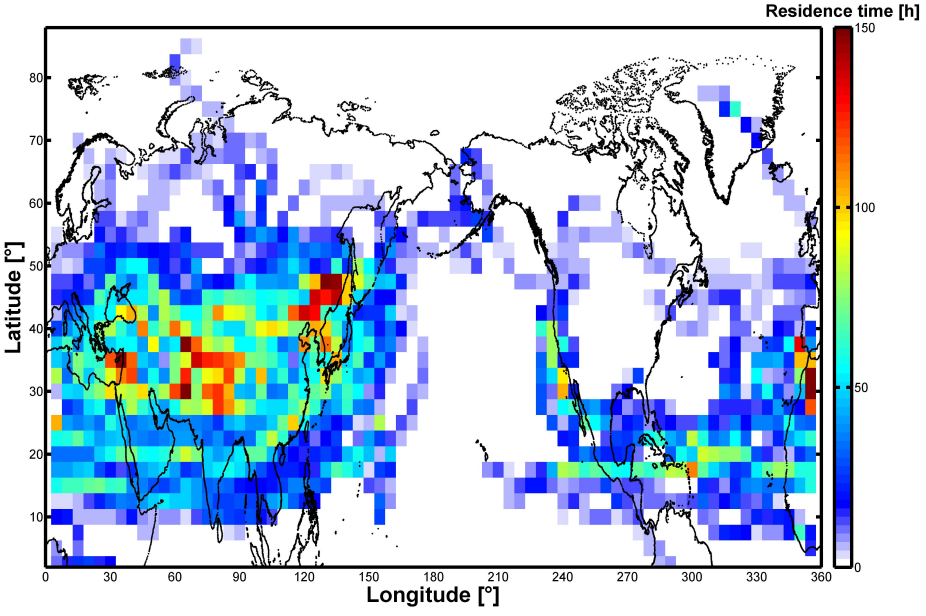

Figure 8. Residence time in hours of the trajectory ensemble as shown in Fig. 6 for -50 days $< t_{Tra} <$ -30 days. (2.5° latitude and 5° longitude bins). Note the long residence time in the ascending region as indicated in Fig. 7.

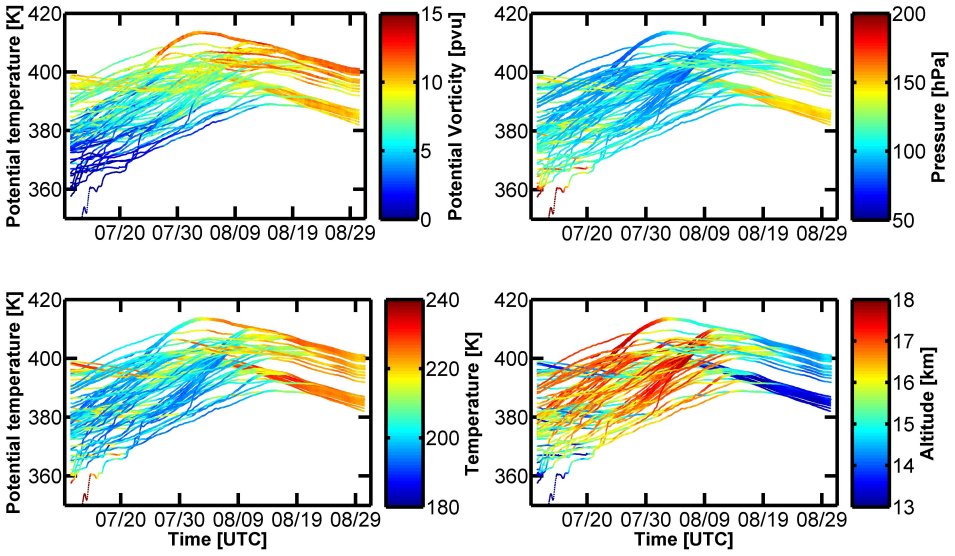

Figure 9. Potential temperature versus time along the trajectory ensemble as shown in Fig. 6. The color indicates the PV (top left), pressure (top right), temperature (bottom left), and altitude (bottom right) based on ERA-Interim reanalysis data.

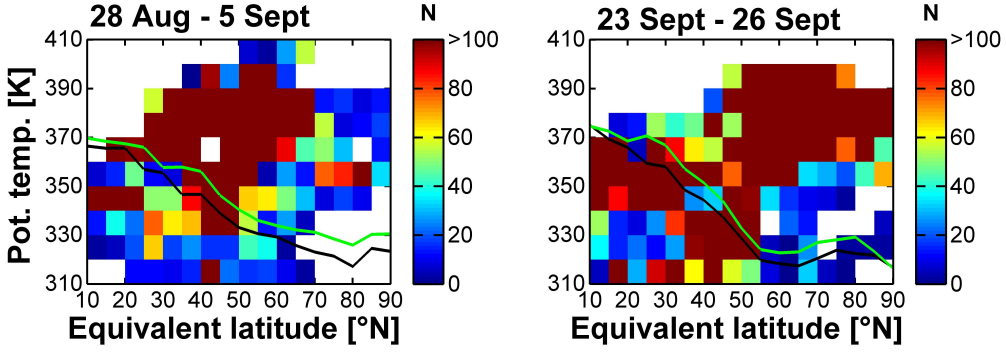

Figure 10. Data coverage (number of data points N in each bin) of TACTS 2012 in potential temperature Θ - equivalent latitude ϕ_{eq} - coordinates. Left: Data coverage of the initial phase of TACTS from the 28 August to 5 September. Right: Data coverage of the final phase of TACTS from the 23 to 26 September. The black and green line denotes the location of the dynamical (PV = 2 pvu) and thermal tropopause (WMO, 1957).

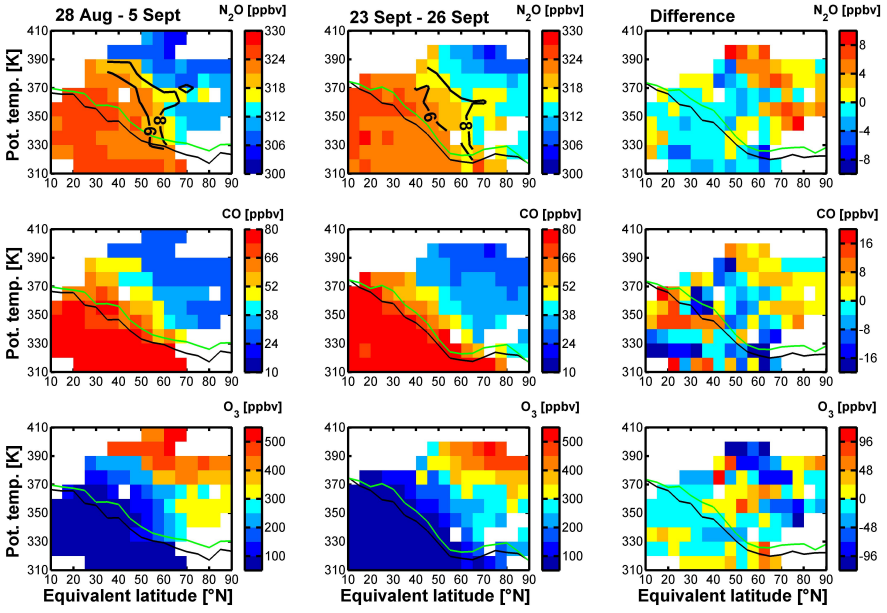

Figure 11. N_2O, CO, and O_3 distributions in potential temperature Θ - equivalent latitude ϕ_{eq} - coordinates for the TACTS 2012 campaign. Left: Distributions for the initial phase of TACTS from the 28 August to 5 September. Center: Distributions for the final phase of TACTS from the 23 to 26 September. Right: Changes in the trace gas distributions during the TACTS 2012 campaign (final minus initial phase). The black and green line denotes the location of the dynamical (PV = 2 pvu) and thermal tropopause (WMO, 1957). The thick black line in the upper array denotes the 6 and 8 pvu isolines calculated from ECMWF data along the flight paths.

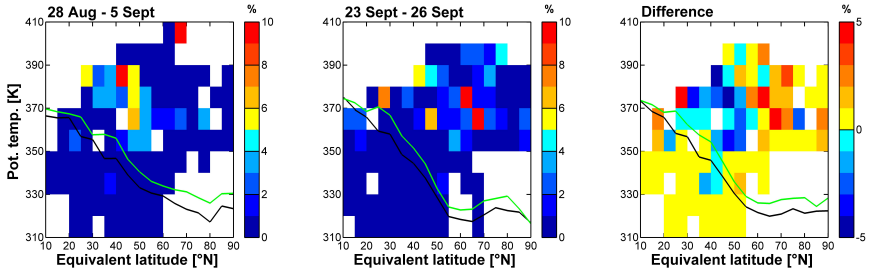

Figure 12. Same presentation as in Fig. 11 but with different color coding. Proportion of data points for which 50 day backward trajectories calculated with CLaMS-TRAJ indicate an origin in the Asian summer monsoon anticyclone (Criterion: 25°N $<$ TRA-latitude $<$ 40°N, 40°E $<$ TRA-longitude $<$ 110°E and Tra-Θ $>$ 360 K for t = -30 days).

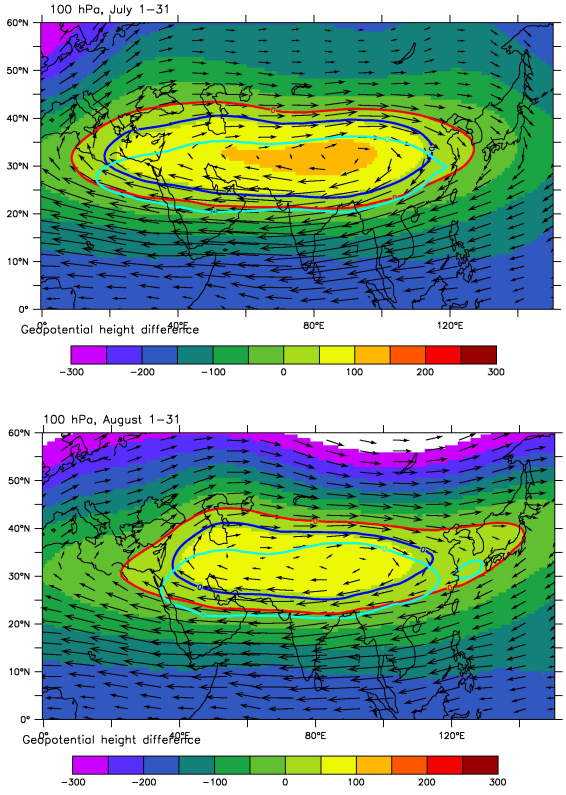

Figure 13. Geopotential height relative to the climatological mean for JJA following the method of Bergman et al. (2013). The dark blue line indicates the monsoon location according to the threshold from Bergman et al. (2013) at 100 hPa (light blue for 200 hPa). The red contour marks the zero line using the mean geopotential height from summer 2012 as threshold to calculate the anomaly.

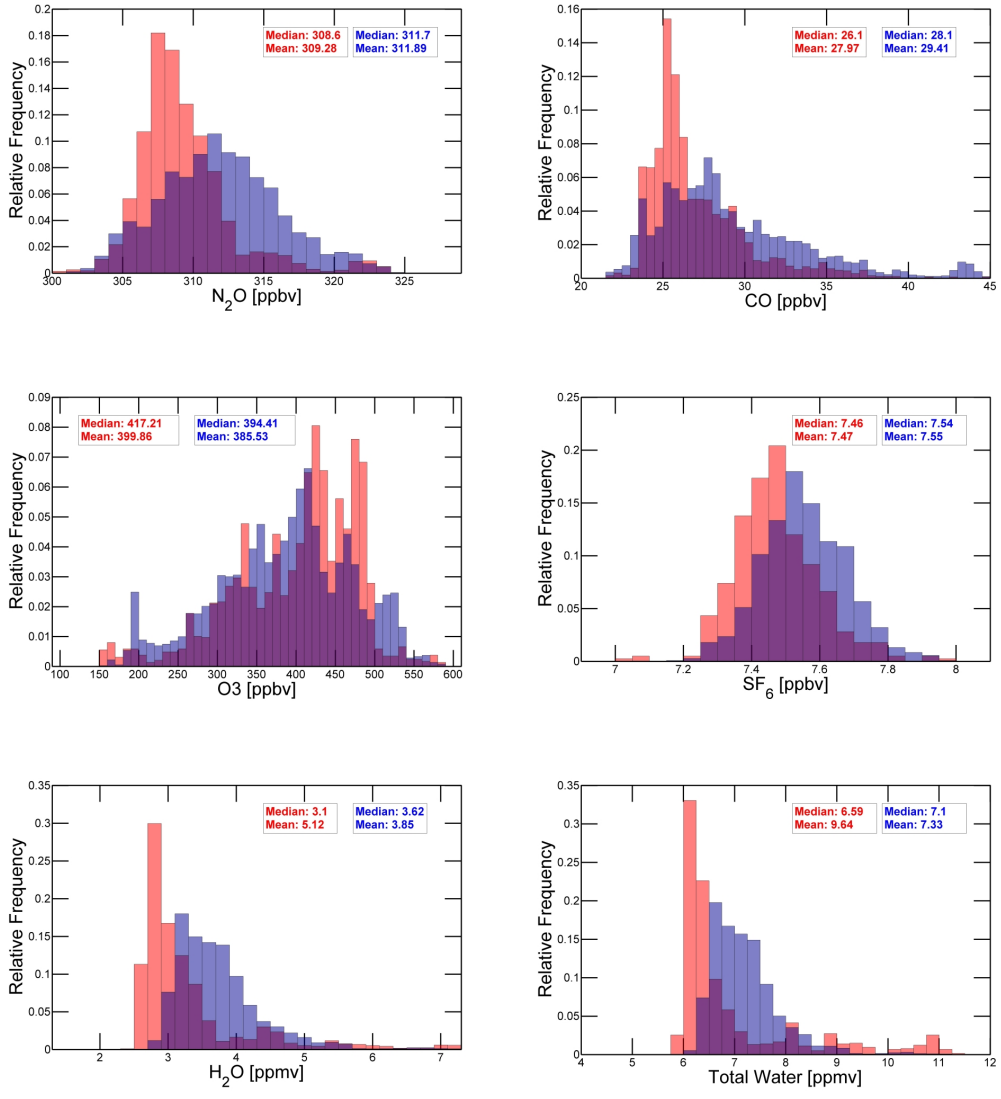

Figure 14. Relative frequency of (a) N_2O, (b) CO, (c) O_3 and (d) SF_6, (e) H_2O, (f) Total Water, for data points with PV > 8 pvu. Redish colors denote the histogram for the initial phase from the 28 August to 5 September, bluish colors for the final phase of TACTS from the 23 to 26 September. Purple areas display the overlap of both histograms.

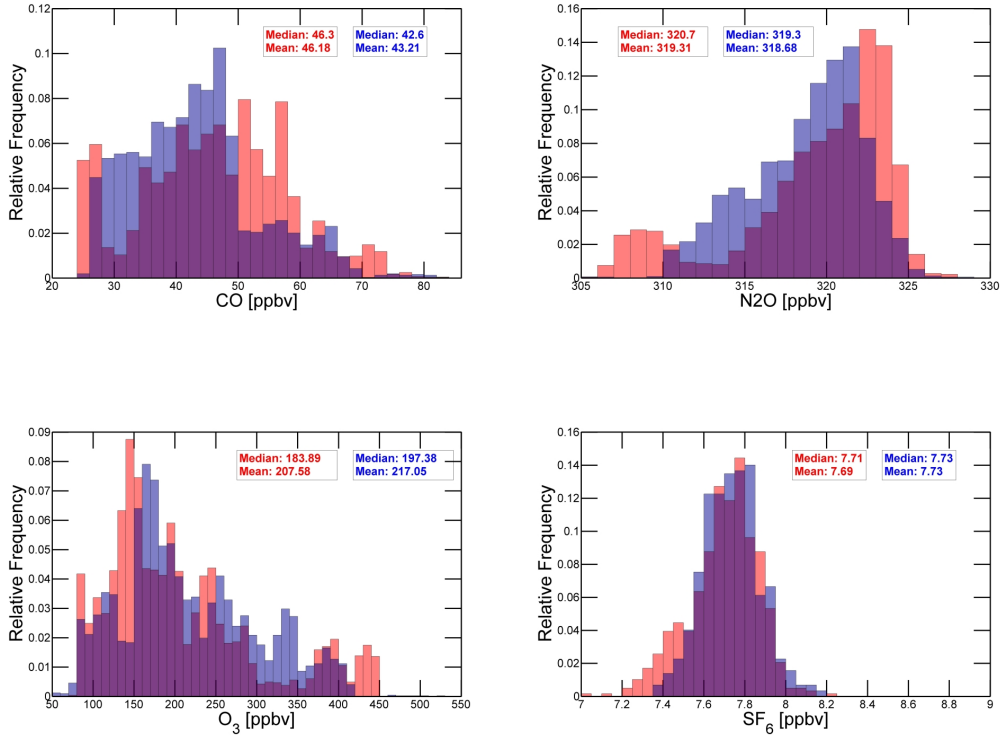

Figure 15. Same as Fig.14 (without H_2O and Total Water histograms) for data points with PV ranging from 3 to 8 pvu.

Table 1. Minimum and maximum values of potential temperature, and CO and O_3 mixing ratios, respectively, for every mixing line. Additonally the number of data points, the flight distance, and R^2 based on a linear regression is listed.

Mixing line	Line 1	Line 2	Line 3	Line 4	Line 5
Θ_{min} [K]	381,5	385,3	377,0	399,0	396,5
Θ_{max} [K]	384,5	389,0	382,0	405,0	401,0
CO_{min} [ppbv]	23,4	23,9	23,7	21,9	23,5
CO_{max} [ppbv]	27,4	28,7	41,4	28,7	28,0
$O_{3\ min}$ [ppbv]	425,59	421,75	248,27	467,82	433,01
$O_{3\ max}$ [ppbv]	485,56	495,11	377,92	583,16	493,54
Date points	71	71	60	65	51
Flight distance [km]	142	142	120	130	102
R^2	0,96	0,96	0,99	0,89	0,96

Table 2. Tropospheric „endmembers“ for every mixing line based on the tracer-tracer-correlations of O_3 and CO, and N_2O and CO, respectively (cf. Fig. 4). The values are based on the intercept between the calculated confidence regions with the assumed mixing ratio of O_3 and N_2O at the tropopause in Fig. 4.

Mixing line	Line 1	Line 2	Line 3	Line 4	Line 5
$R_{Trop}(O_3)$= 100 ppbv					
CO_{min} [ppbv]	42,0	45,9	59,3	47,2	44,5
CO_{max} [ppbv]	50,9	52,7	62,2	54,0	55,1
$R_{Trop}(N_2O)$= 325 ppbv					
CO_{min} [ppbv]	35,1	35,4	54,1	38,8	35,2
CO_{max} [ppbv]	44,2	39,8	68,0	46,2	47,3